HHS Public Access

Author manuscript

Eur J Neurosci. Author manuscript; available in PMC 2016 December 08.

Published in final edited form as:

Eur J Neurosci. 2015 December ; 42(12): 3018–3032. doi:10.1111/ejn.13083.

Localization and expression of GABA transporters in the suprachiasmatic nucleus

Michael Moldavan[1], **Olga Cravetchi**[1], **Melissa Williams**[3], **Robert P. Irwin**[1], **Sue A. Aicher**[3], and **Charles N. Allen**[1,2]

[1]Oregon Institute of Occupational Health Sciences, Oregon Health & Science University, 3181 S.W. Sam Jackson Park Road, Portland, Oregon 97239-3098, USA

[2]Department of Behavioral Neuroscience, Oregon Health & Science University, 3181 S.W. Sam Jackson Park Road, Portland, Oregon 97239-3098, USA

[3]Department of Physiology and Pharmacology, Oregon Health & Science University, 3181 S.W. Sam Jackson Park Road, Portland, Oregon 97239-3098, USA

Abstract

GABA is a principal neurotransmitter in the suprachiasmatic hypothalamic nucleus (SCN), the master circadian clock. Despite the importance of GABA and GABA uptake for functioning of the circadian pacemaker, the localization and expression of GABA transporters (GATs) in the SCN has not been investigated. The present studies used Western blot analysis, immunohistochemistry, and electron microscopy to demonstrate the presence of GABA transporter 1 (GAT1) and GABA transporter 3 (GAT3) in the SCN. By light microscopy, GAT1 and GAT3 were co-localized throughout the SCN, but were not expressed in the perikarya of arginine vasopressin- or vasoactive intestinal peptide-immunoreactive (−ir) neurons of adult rats, nor in the neuronal processes labeled with the Neurofilament Heavy Chain. By electron microscopy, GAT1- and GAT3-ir was found in glial processes surrounding unlabeled neuronal perikarya, axons, dendrites, and enveloped symmetric and asymmetric axo-dendritic synapses. Glial Fibrillary Acidic Protein-ir astrocytes grown in cell culture were immunopositive for GAT1 and GAT3 – and both GATs could be observed in the same glial cell. These data demonstrate that synapses in the SCN function as “tripartite” synapses consisting of presynaptic axon terminals, postsynaptic membranes, and astrocytes that contain GABA transporters. This model suggests that astrocytes expressing both GATs may regulate the extracellular GABA, and thereby modulate the activity of neuronal networks in the SCN.

Address for correspondence: Charles N. Allen, Ph.D., Occ. Health Sci., L606, Oregon Health & Science University, Portland, OR 97239-3098, Phone: (503) 494-2507, Fax: (503) 494-6831, allenc@ohsu.edu.

Authors’ contributions

MM and CNA conceived and designed the experiments, MM collected, and analyzed the data. MM and CNA interpreted the data and wrote, and revised the manuscript. OC and MM collected and analyzed WB and IHC data, processed the images. OC and RPI prepared the SCN cell cultures. TEM imaging and analysis were done by MW and SAA. All authors read and approved the final version of the manuscript.

Conflict of Interests

The authors declare that there are no conflicts of interests regarding the publication of this manuscript.

Keywords

GABA transporter; suprachiasmatic nucleus; hypothalamus; immunohistochemistry; Western blot; electron microscopic imaging; circadian rhythm

INTRODUCTION

GABA is the most abundant neurotransmitter in the suprachiasmatic nucleus (SCN), where it regulates many functions, including light-induced phase shifts, synchronization of the dorsal and ventral SCN, synchronization of the circadian phase of individual SCN neurons, and the sensitivity of the circadian clock to light-entraining signals (Ralph & Menaker, 1985; Moore & Speh, 1993; Wagner *et al.*, 1997; Albus *et al.*, 2005; Aton *et al.*, 2006; Belenky *et al.*, 2008; Moldavan & Allen, 2013). GABA content, glutamic acid decarboxylase (GAD) activity and mRNA levels, GABAergic synaptic transmission, and $GABA_B$ receptor-mediated presynaptic inhibition of the retinal input to the SCN demonstrate circadian rhythmicity (Cattabeni *et al.*, 1978; Aguilar-Roblero *et al.*, 1993; Huhman *et al.*, 1996; Wagner *et al.*, 1997; Cardinali & Golombek, 1998; De Jeu & Pennartz, 2002; Gompf & Allen, 2004; Itri *et al.*, 2004; Moldavan & Allen, 2013). GABA's action on synaptic and extrasynaptic receptors is terminated by diffusion from the synaptic cleft, the GABA uptake into presynaptic nerve terminals, or uptake into surrounding astrocytes (Madsen *et al.*, 2010). There are four specific high-affinity Na^+/Cl^- dependent GABA transporters: GABA transporter 1 (GAT1), GABA transporter 2 (GAT2), GABA transporter 3 (GAT3), and betaine/GABA transporter (Borden, 1996; Scimemi, 2014). GAT1 and GAT3 are expressed in the brain and show region and cell-type specific localization patterns (Itouji *et al.*, 1996; Ribak *et al.*, 1996a; Jin *et al.*, 2011). In the majority of brain structures, GAT1 and GAT3 are localized to astrocytes, and only GAT1 has been found in axon terminals (Minelli *et al.*, 1995; Minelli *et al.*, 1996; Ribak *et al.*, 1996b; De Biasi *et al.*, 1998; Jin *et al.*, 2011).

In the SCN, the GABA uptake inhibitors nipecotic acid and riluzole increase arginine vasopressin (AVP) release (Isobe & Nishino, 1997). The GABA that accumulates during application of nipecotic acid activates $GABA_B$ receptors and inhibits glutamate release from retinohypothalamic tract (RHT) synapses (Moldavan & Allen, 2013). Despite the importance of GABA uptake for GABAergic neurotransmission, the expression and localization of GATs in the SCN have not been described in detail.

The aim of this study was to determine the types of GABA transporters expressed in the SCN, their diurnal expression pattern, and their cellular localization. We found that both GAT1 and GAT3 are expressed in the SCN, but did not exhibit significant rhythmic changes in diurnal expression. Detectable GAT1- and GAT3-ir were found only in glial processes surrounding unlabeled neuronal perikarya and axo-dendritic synapses. Our data indicate an important role for GAT1- and GAT3-expressing glial cells in regulating GABA uptake in the SCN.

METHODS

The Institutional Animal Care and Use Committee of Oregon Health & Science University approved in advance all the experimental procedures involving animals. Animal handling was conducted in accordance with National Institutes of Health Guide for Care and Use of Laboratory Animals and associated guidelines. All efforts were made to minimize pain and the number of animals used.

Animals and housing

Four to six weeks old male Sprague-Dawley rats (Charles River Labs, Wilmington, MA) were housed in an environmental chamber (Percival Scientific, Perry, IA) maintained at 21°C on a 12:12 hr light:dark (LD) cycle, with free access to food and water. These animals were used for the Western blot, immunohistochemistry and electron microscopy studies. Pregnant female Sprague-Dawley rats (19 - 20 days gestation) were purchased from Charles River Labs (Wilmington, MA). The female rats were housed in an environmental chamber (Percival Scientific, Perry, IA) maintained at 21°C on a 12:12 hr light:dark (LD) cycle, with free access to food and water. Zeitgeber time was used to define light and dark phases during the LD cycle. By convention, ZT12 was defined as lights-off.

Brain tissue collection for Western blots

Rats were deeply anesthetized with isoflurane (Hospira, Inc, Lake Forest, IL), brains were removed and submerged in an ice-cold Krebs solution consisting of (in mM): NaCl 82.7, KCl 2.4, $CaCl_2$ 0.5, MgCl2 6.8, NaH_2PO_4 1.4, $NaHCO_3$ 23.8, dextrose 23.7, sucrose 60, saturated with 95% O_2 and 5% CO_2; pH 7.3 - 7.4; 308 - 310 mOsm (Mathews *et al.*, 2012). Coronal brain slices (250 μM thick) were cut with a vibrating-blade microtome (Leica VT 1000 S, Leica Biosystems Nussloch GmbH, Germany) (Moldavan & Allen, 2013). Olfactory bulb, cerebral cortex and cerebellum were trimmed off, and separately homogenized after the meninges were removed. Hippocampus, striatum, thalamus, and hypothalamus (without SCN) were cut from the brain slices, and the retina was extracted from the eye with a fine sharp razor blade. Samples were collected at ZT 6 – 8. During a single collection period about 20 slices containing the SCN were cut from 10 rats, then transferred into a chamber with ACSF, kept at 30°C and bubbled with carbogen (5% CO_2 & 95% O_2). Each lobe of the bilateral SCN was “punched” out of the slice in ice-cold ACSF with a Harris Uni-Core Hole puncher (inner diameter 0.5 mm; Ted Pella, Inc.; Redding, CA). To increase the protein yield in the sample, we tried to minimize the amount of ACSF that remained with the collected tissue. To accomplish this, the SCN punches were pricked with a glass micropipette with a 10 mm long fine tip and transferred to an eppendorf tube filled with ice-cold lysis buffer (RIPA with the protease inhibitors/PMSF). During one collection period about 40 punches were collected from 10 rats, and the punching procedure took 1.5 - 2 hours. The collection procedure was repeated twice for each ZT, and in total the tissue from 20 rats was collected for each ZT. To study the diurnal GAT expression, the SCN tissue samples were collected at: ZT 4 - 6, ZT 8 - 10, ZT 14 - 16, ZT 18 - 20, and ZT 22 - 24. The punching procedure for each ZT took 1.5 - 2 hours. The circadian clock continues to run and retains the initial phase after brain slices were cut and placed into ACSF under physiological conditions (Green & Gillette, 1982; Groos & Hendriks, 1982; Shibata *et al.*, 1982; Gillette,

1986; vanderLeest *et al*., 2009). Consequently, the SCN circadian clock function was fixed and GATs expression was preserved for a specified ZT.

Western blot procedures and data analysis

Tissue samples of SCN, olfactory bulb, cerebral cortex, cerebellum, retina, hippocampus, striatum, thalamus, and hypothalamus were collected as described above. The tissue was homogenized in twenty volumes of ice-cold RIPA buffer with protease inhibitors/PMSF (homogenizer - Kontes Pellet Pestle Cordless Motor, #K749540-0000 with adapter, Fisher Scientific, Pittsburgh, PA), centrifuged (12,000×g, for 10 min at 4°C) and the supernatant collected. A Bradford assay (#500-0006, Bio-Rad protein Assay Dye Reagent Concentrate, Life Science Research, Hercules, CA) was used to determine the total protein concentration in the samples. The absorbance of bovine serum albumin (BSA) standard (B9001S or B9000S, New England BioLabs) and lysate samples was measured at 595 nm in duplicates with a Shimadzu UV-1700 PharmaSpec Spectrophotometer (Shimadzu Scientific Instruments, MD). A standard curve with serial dilutions of BSA was drawn, and the total amount of protein in each lysate was calculated. The volume of lysate containing equal amounts of protein was calculated for each sample. Reduced samples (5 μg of protein/20 μl per well) were loaded into 4-12% precast Bis-Tris gels (Life Technologies, Grand Island, NY). During the SDS-PAGE routine, the samples of SCN tissue, that represented different ZTs, were run simultaneously on the same gel. To reduce any systematic error that may appear during the proteins' run or transfer, the samples were placed into wells in different sequences for each new gel. The proteins were SDS-PAGE separated at 125V and electroblotted (40V for 1 hour) onto PVDF membranes. For the ECL detection, the blots were blocked in 5% non-fat milk/TBST and incubated with a rabbit anti-GAT1 polyclonal antibody (AGT-001, Alomone Labs Ltd., Jerusalem, Israel, 1:500) overnight at 4°C in the same buffer with agitation. A donkey polyclonal anti-rabbit IgG-HRP conjugated secondary antibody (sc-2313, Santa Cruz Biotechnology Inc., Santa Cruz, CA, 1:5000) was added for 1 hr at RT. For a loading control a mouse anti-Glyceraldehyde-3-Phosphate Dehydrogenase (GAPDH) purified monoclonal antibody (MAB374, Millipore, Temecula, CA, 1:8000) was applied followed by rabbit polyclonal anti-mouse IgG-HRP conjugated secondary antibody (AP160P, Millipore, 1:200,000). A molecular mass marker (kDa) was applied (# 161-0374, Bio-Rad, Life Science Research). The bands were detected on the X-ray film following the incubation with a chemiluminescent substrate (PI-34077, Thermo Scientific, Rockford, IL). For GAT3 detection, the blots were blocked and incubated overnight in Odyssey blocking buffer containing a rabbit anti-GAT3 polyclonal antibody (AB1574, Millipore, 1:1000). The secondary antibody was a goat anti-rabbit IRDye 680conjugated IgG (# 926-32221, LI-COR Biosciences, 1: 4000, channel 700 nm, red) with 1 hr incubation time. For loading control, a mouse anti-GAPDH monoclonal antibody (1:8000) was applied followed by IRDye 800CW Goat Anti-Mouse conjugated IgG (# 926-32210, LI-COR Biosciences, 1: 3000, channel 800 nm, green) secondary antibody.

The blot image was taken and the optical density (O.D.) was determined for each sample. GAT1 blots were scanned from X-ray film. GAT3 blots were processed with Odyssey infrared imaging system (densitometer Odyssey, LI-COR Biosciences, Lincoln, NE). The optimal exposure was chosen to avoid the saturation of the image. For each sample the O.D.

of the GAT1 or GAT3 band was quantified with ImageJ (National Institutes of Health), normalized to the corresponding loading control, then averaged across all gels. The GAT expression in different brain regions was compared to the GAT expression in the SCN and the data presented in ratio units (5 gels/graph, mean ± SE). The GATs expression in different brain regions versus expression in the SCN was analyzed using a Student's t-test.

The O.D. of GAT1 and GAT3 bands were measured at each of five ZTs, normalized to the corresponding loading control, averaged for all gels, and plotted. The JTK_Cycle nonparametric algorithm was used to determine if there were diurnal changes of GAT1 and GAT3 expression (Hughes *et al*., 2010). Data are presented as means ± S.E.M. KaleidaGraph TM (version 3.6; Synergy Software, Reading, PA), Excel 11.6.5 (or 14.1.3) (Microsoft Co., Redmond, WA), FreeHand MX (Macromedia, Inc, San Francisco, CA), JTK_Cycle (http://openwetware.org/wiki/HughesLab:JTK_Cycle), and R (V3.02 R Development Core Team, www.R-project.org) were used for curve fitting, data analysis and graphic presentation.

Immunohistochemistry

Each rat was deeply anaesthetized with isoflurane and transcardially perfused with phosphate buffered saline 1× (PBS), pH 7.4, followed by 4% paraformaldehyde (PFA) in PBS. After perfusion, the brain was post-fixed in PFA for 18 hours at 4°C and cryoprotected by incubating overnight at 4°C first in 10% then 30% sucrose in PBS. Brain blocks were embedded in Shandon Cryochrome embedding medium (Thermo Fisher Scientific Inc., Waltham, MA) and fast-frozen by dry ice mixed with 96% ethanol for 3-5 minutes. Coronal (20 μm thick) sections were cut with a Leica cryostat (CM1950, Leica Microsystems, Inc., Buffalo Grove, IL), thaw-mounted onto pre-cleaned SuperFrost® Plus glass slides, and dried at 37°C. Air-dried SCN-containing sections were hydrated in 0.1 M PB. To reduce background autofluorescence, the sections were incubated in an aldehyde-reducing agent 1% $NaBH_4$ in 0.1 M PB for 30 min and rinsed copiously with multiple changes of 0.1 M PB until there were no signs of bubbles (Luquin *et al.*, 2010). The tissue was permeabilized with 0.3% Triton X-100 in TBS and non-specific binding was blocked by incubation in 5% normal donkey serum for 1 h at RT.

To study GAT1 expression alone, sections were incubated with the rabbit anti-GAT1 polyclonal antibodies AB1570 (Millipore, Temecula, CA, 1:100) or ab72448 (Abcam, Inc., Cambridge, MA, 1:500). GAT3 expression was studied by application of a rabbit anti-GAT3 polyclonal antibody (AB1574, Millipore, 1:100 or 1:500). For dual-labeling experiments, GAT1 or GAT3 antibodies were applied with different cellular markers (see Table 1). After an overnight incubation at 4°C sections were washed with 0.3% TX/TBS. A complete list of antibodies and concentrations used is shown in Table 1. Samples were counterstained with 300 nM DAPI (D1306, Molecular Probes, Eugene, OR) in 0.1 M PB. Sections were rinsed, and coverslipped with ProLong Gold antifade mounting media (P36934, Life Technologies).

Controls for antibody specificity

Western blot—Positive control: control peptide antigen (supplied with AGT-001, Alomone Labs) was used to verify the specificity of bands detected with the GAT1

antibody. GAT1 band disappeared when antibody was preadsorbed overnight in excess of blocking peptide (antibody/antigen ratio 1:5). The positive control for GAT1 was a cerebral cortex lysate, for GAT3 - thalamus lysate. The specificity of GAT3 antibody (cat no. AB1574; Millipore, Temecula, CA) was previously determined using immunoblot analysis with antigen preabsorption (Ikegaki *et al.*, 1994; Ribak *et al.*, 1996b). The negative control was loading buffer without sample. The loading control was GAPDH.

IHC—For a negative control the primary antibodies were substituted with the host's species IgG that completely abolished the immunostaining. The positive control for GAT1 was cerebral cortex tissue.

Imaging

Images were taken with a Zeiss Axioskop 2 TM fluorescent microscope using AxioVision 4.8 software (Carl Zeiss MicroImaging, Inc.). The images of double-labeled immunofluorescent tissue sections were acquired on laser scanning confocal microscope systems: Olympus Fluoview FV1000 (FV10-ASW 3.1b software) or on a Zeiss LSM 780 (Zeiss ZEN 2011 acquisition software; Carl Zeiss MicroImaging, Inc.). Similar results were produced from both confocal microscope systems. Confocal micrographs consisted of several 0.4 μm thick optical sections adjusted for optimal brightness and contrast using FIJI software.

Electron Microscopy (EM) Immunocytochemistry for Gold Labeling

Perfusion and tissue preparation for immunocytochemistry—Rats were anaesthetized with pentobarbital sodium (150 mg/kg) and perfused transcardially through the ascending aorta with 5-10 mL of heparinized saline (1000 U/mL), followed by 50 mL of 3.8% acrolein in 2% paraformaldehyde (PFA), followed by 200 mL of 2% PFA in 0.1 M PB, pH 7.4 (Aicher *et al.*, 2003b). Immediately following perfusion, brains were removed and blocks of tissue containing SCN were placed in 2% PFA for 30 min before being transferred to 0.1 M PB. Blocks of tissue were stabilized in agar and sectioned coronally on a vibrating microtome (Leica Microsystems, Inc., Buffalo Grove, IL) at 40 μm. Alternate sections were collected and processed for GAT1 and GAT3 immunocytochemistry, respectively.

Immunocytochemistry for EM studies—The following pre-treatments were performed in sequence: To bind remaining free aldehydes and increase the antigenicity of acrolein-perfused tissues, sections were incubated in 1% $NaBH_4$ (Sigma–Aldrich) in 0.1 M PB for 30 min; to increase membrane permeability of the antibody solutions for EM, sections were cryoprotected in a 25% sucrose 1% glycerol solution for 15 minutes then rapidly immersed sequentially for a few seconds each in liquid Freon (Freon 22) and liquid nitrogen before being transferred back to 0.1 M PB; and finally to reduce non-specific binding, tissue was incubated for 30 minutes in 0.5% BSA in 0.1 M Tris saline, pH 7.6, then washed in 0.1 M Tris.

Following these pre-treatments, sections were incubated in either rabbit anti-GAT1 primary antibody (ab72448, Abcam) or rabbit anti-GAT3 primary antibody (AB1574, Millipore)

diluted 1:50 in 0.1 M Tris buffer, pH 7.6 for 48 hours at 4°C. Following primary antibody incubation, all sections were buffer washed and incubated in goat anti-rabbit gold conjugated IgG (EMS, 25101) diluted 1:50 in a white fish gelatin/BSA solution in 0.01M PBS for 2 hours at room temperature. Sections were then incubated in 2% EM grade glutaraldehyde for 10 minutes; citrate buffer washed and silver intensified using the IntenSE™ M kit (GE Healthcare Life Sciences, Buckinghamshire, UK).

Electron microscopy—Following immunolabeling, tissue sections were fixed for 15 minutes in 1.0% osmium tetroxide, dehydrated and flat embedded in EMBed-812 (EMS, RT 14120) between two sheets of ACLAR plastic (EMS, 50425) and cured in a 60°C oven for 24 – 48 hrs. Regions of tissue containing labeled cells were glued onto cured resin blanks and 70 nm sections were cut on an ultramicrotome (Leica Microsystems, Inc.), picked up on copper grids, and counterstained with uranyl acetate and Reynold's lead citrate. Areas of interest containing immunogold labeling at the tissue/plastic interface were examined on an FEI Tecnai BioTwin electron microscope at 80 kV. Criteria for positive immunogold labeling were similar to previous descriptions (Aicher *et al.*, 2003a).

SCN primary cell culture preparation

Prior to the cell isolation, 35 mm dishes with a 14 mm glass bottom (Cat # P35G-0-14-C, Mattek Corp., Ashland, MA,) were coated with 0.4% Polyethylene imine (Cat # 03880, Sigma-Aldrich Fluka, St. Louis, MO) in 0.1 M Borate buffer (Lelong *et al.*, 1992), with cell culture inserts (Cat # 80209, Ibidi LLC., Verona, WI) attached to the center of the glass bottom for each 35 mm dish. Rat glial cells were prepared as described in Kaech and Banker (Kaech & Banker, 2006) and plated on the dishes outside the Ibidi inserts and grown to about 80% confluence in MEM (# 11095-080, Life Technologies), supplemented with 10% horse serum, 20% D-Glucose (19 mM final) and penicillin/streptomycin 1:100. One day before the SCN cell preparation, the media was replaced with MEM+ 5% FBS and returned to the incubator overnight.

The SCN cells were obtained under aseptic conditions from one-day rat pups (Charles River) euthanized by rapid decapitation. The brains were rapidly removed and placed into ice cold slicing buffer: 1× HBSS (with Ca^{2+}, Mg^{2+} without $NaHCO_3$; Cat # 14065, Life Technologies), supplemented with 1M HEPES (0.01 M final), $NaHCO_3$ (4.2 mM final) and penicillin/streptomycin 1:100. The osmolarity of the slicing buffer was 285-315 mOsm. Forebrains were cut preserving the hypothalamus, and secured onto a vibratome stand using a cyanoacrylate adhesive (Cat # 14037127414, Leica Biosystems, Buffalo Grove, IL). Coronal slices 300 μm thick were cut at the level of the optic chiasm, using a vibrating blade microtome (VT1000 S, Leica Biosystems, Buffalo Grove, IL Cat# VT1000 S). The slices were examined under a dissecting microscope, and SCN nuclei were punched using an 18-gauge blunt needle (Cat # B18-100, SAI, Lake Villa, IL). The punches were transferred into a sterile conical 1.5 ml tube with dissociation media: 1× HBSS (without Ca^{2+}, Mg^{2+}; Cat # 14185, Life Technologies), supplemented with 1M HEPES, 3.6 g/L D-Glucose and penicillin/streptomycin. The tissue pieces were washed of any leftover slicing buffer by spinning the tube at 1000 rpm in a microcentrifuge. Next, the tissue was enzymatically digested for 15 minutes at 37°C using > 20 units/ml papain solution (Cat # LK003176,

Worthington Corp., Lakewood, NJ), previously dissolved and activated in HBSS containing 1.1 mM EDTA, 0.067 mM mercaptoethanol and 5.5 mM cysteine (Huettner & Baughman, 1986). After the digestion solution was aspirated off, the tissue was resuspended in conditioned SCN plating media (MEM + 5% FBS) in a volume ≈100 μl per one SCN punch. The suspended tissue was then gently triturated using a fire polished Pasteur pipette avoiding air bubble formation. The SCN cells were transferred in 80 μL of plating media into each chamber of the Ibidi insert (Ren & Miller, 2003). After 3-4 hours of incubation at 37°C, which allowed time for the SCN cells to attach to the coated glass bottom, the Ibidi inserts were removed from each dish. The plating media was gradually replaced by MEM (Cat # 11095-080, Life Technologies,) with addition of N-2 supplement (Cat # 11095-080, Life Technologies), 5% FBS, 20% D-Glucose (19 mM final) and penicillin/streptomycin 1: 100. After one week in culture the cells were washed of the media with 1× HBSS (with Ca^{2+}, Mg^{2+} without $NaHCO_3$; Cat # 14065, Life Technologies) and fixed with 4% paraformaldehyde in 0.1 M PB.

Fluorescent Immunocytochemistry and Imaging of SCN cell cultures—The fixed SCN cultured cells were washed of fixative in Ca^{2+} & Mg^{2+} containing HBSS. The paraformaldehyde residue was quenched with 0.1 M glycine in HBSS for 30 minutes. Washed cells were permeabilized in 0.3% TritonX containing HBSS and non-specific blocking was subsequently performed with 5% donkey serum. To study GAT1 and GAT3 expression in astrocytes, either a rabbit anti-GAT1 antibody (ab426, Abcam, 1:500) or a rabbit polyclonal anti-GAT3 antibody (AB1574, Millipore, 1: 250) were combined with a mouse monoclonal IgG to glial fibrillary acidic protein (GFAP, MAB3402, Millipore, 1: 250). For the GAT-1 co-localization with the GAT-3 the mouse monoclonal anti-GAT-3 antibody (sc-376001, Santa Cruz Biotechnology, 1; 250) was used in combination with the rabbit anti-GAT1 antibody (Abcam ab426, 1: 500). The cultured cells were incubated with the primary antibodies overnight at 4°C. Following washes with 0.3% TritonX in 1× HBSS (with Ca^{2+} and Mg^{2+}) the secondary detection was carried out using a mixture of 1:500 donkey anti-rabbit DyLight 550 (ab96920, Abcam) and 1:250 donkey anti-mouse DyLight 488 (#715-546-151, Jackson ImmunoResearch) conjugated antibodies for 4 hours at room temperature. After subsequent washes the nuclei were counterstained with 300 nM DAPI (D1306, Life Technolodies) in HBSS. The culture dishes were washed and filled with 1 ml of HBSS for imaging.

To determine the autofluorescence level only the secondary antibody was applied (isotype control). Cell culture images were captured with a Nikon Eclipse Ti inverted confocal microscope (Nikon Instruments Inc.) equipped with CSU-W1 confocal scanner unit (Yokogama Electric Corp.) using software NIS-Elements AR 3.0.

RESULTS

Western blot analysis

a) Comparison of GAT1 and GAT3 expression in SCN and other brain regions —Western blot analysis was used to determine the expression pattern of GATs in the SCN and other brain regions. A band for GAT1 was observed at ~67 kDa (Fig. 1A, *top*). The

optical density (O.D.) was measured, normalized to loading control (see *Methods*) and GAT1 expression in several brain regions was compared to the expression level in the SCN (Fig. 1A, *bottom*). The highest GAT1 expression was observed in the cerebral cortex. The normalized optical density (O.D.n.) ratios for cerebral cortex and hippocampus versus SCN were 2.1 (Student's paired t-test, two-tail, $P < 0.01$, n = 5 gels) and 1.4 ($P < 0.05$, n = 5), respectively. GAT1 expression was similar in cerebellum, striatum, thalamus, hypothalamus, and SCN. The olfactory bulb and retina had significantly lower GAT1 expression (O.D.n. 0.4 and 0.5 of the SCN value, respectively, $P < 0.001$, n = 5). The cerebral cortex lysate was used as a positive control because of the high level of GAT1 expression. To confirm the antibody specificity, the anti-GAT1 antibody was applied in duplicates to the cerebral cortex sample with and without a blocking peptide (Fig. 1A, *bottom, insert).* GAT3 expression was highest in the thalamus, hypothalamus and SCN (Fig. 1). In other brain regions studied, GAT3 expression was significantly lower ($P < 0.001$, n = 5 gels). The O.D.n. measured for olfactory bulb was 0.77 of that observed in the SCN. For cerebral cortex, cerebellum, retina, hippocampus and striatum the O.D.n. did not exceed 0.2 of the SCN value (Fig. 1B).

b) Studies of diurnal rhythmicity of GAT1 and GAT3 expression in the SCN— We tested the hypothesis that GAT1 and GAT3 demonstrate a diurnal rhythmic expression in the SCN. Adult male rats were maintained on a 12:12 hr LD cycle for at least a week. The rats were sacrificed, brain slices prepared, and SCN tissue collected during ZT 4 - 6, ZT 8 - 10, ZT 14 - 16, ZT 18 - 20, and ZT 22 - 24. Western blot procedures were applied to samples (see *Methods* and Table 1, Fig. 2A, B). To quantify the data, O.D. was measured for each band, normalized to the loading control value, and plotted (Fig. 2 C). Neither GAT1 nor GAT3 expression showed significant changes over the 24 hour period (the permutation based p values ADJ.P were 1 for both GAT1 and GAT3) (Hughes *et al*., 2010).

Immunohistochemical studies of GAT1 and GAT3

Light microscopic images showed the heaviest GAT1 immunostaining in the hypothalamus between the lobes of the SCN and around the third ventricle (Fig. 3). However, fairly even GAT1 immunofluorescence was observed throughout the SCN (Fig. 3A, B). Sections were counterstained with DAPI to determine the location of cell nuclei and the contour of the SCN (Fig. 3B). The cerebral cortex was used as a positive control because of abundant GAT1 expression (data not shown). Interestingly, high-resolution immunofluorescent images revealed punctate GAT1 labeling encircling cell perikarya in the SCN (Fig. 3C). GAT1-ir outlined a dense neuropil surrounding unlabeled cell bodies presumably belonging to neurons (Fig. 3D). Therefore, we conducted electron microscopic studies to determine, if GAT1 is expressed in the neurons or in glial cells (see below).

Several neuronal markers were used in an attempt to determine whether SCN neurons express GATs. Antibodies to Neuronal nuclear antigen (NeuN) and to Neuron Specific Enolase (NSE) stained SCN neurons weakly (data not shown). An anti-Neurofilament Heavy chain 200 kDa (NFH) antibody was used to stain neurofilaments, which are the major component of the neuronal cytoskeleton providing structural support to the axon. A dense network formed by NFH-ir neuronal processes was observed in the SCN (Fig. 3E, F).

GAT1-immunolabeling closely followed the pattern of intertwined neuronal processes immunopositive to NFH, which surrounded unlabeled perikarya (Fig. 3F) but dual-labeled profiles were not observed. GFAP-ir astrocytes were detected by application of anti-GFAP antibody (Fig. 3G - I). Large processes of GFAP-immunopositive astrocytes were encompassed by GAT1 expressing tissue (Fig. 3I). The merged images showed occasional co-localization of GAT1- and GFAP-immunostaining. The density of GFAP-positive astrocytes appeared to be higher in the ventrolateral part of the SCN, around the third ventricle, between the lobes of the SCN (Fig. 3G), in contrast to the fairly even GAT1 immunostaining. Immunocytochemistry confirmed the localization of GAT3 in the SCN and surrounding hypothalamic tissue (Fig. 4A, B). The neuronal processes immunopositive for NFH (Fig. 4 D, E) were in close proximity to GAT3-ir profiles. NFH-ir was much stronger in the ventral part of the SCN and did not show co-localization with GAT3 immunostaining (Fig. 4C). GAT3-ir was also observed in the SCN regions where GFAP-ir was poorly expressed or was not detected (Fig. 4F). GFAP-ir astrocytic processes were surrounded by tissue immunolabeled for GAT3 (Fig. 4G, H). GAT3 expressed fairly evenly in the SCN and surrounding hypothalamic region in contrast to the expression of GFAP-positive astrocytes, which had a higher density in the ventrolateral part of the SCN, between the lobes of the SCN, and in the optic chiasm (Fig. 4F). GAT3-ir was not observed in the neuronal perikarya labeled with antibodies to arginine vasopressin (AVP) (Fig. 5A - C) or to vasoactive intestinal peptide (VIP) (Fig. 5G - I). GAT1-ir also was not detected in the perikarya of neurons labeled for AVP (Fig. 5D - F). Double staining with antibodies to GAT1 and GAT3 showed a significant co-localization of these two transporters (Fig. 6). Our further studies using cell culture revealed that GAT1 and GAT3 are co-expressed in the same glial cell (see below).

Thus, our immunohistochemical data indicate that GAT1 and GAT3 were not expressed in AVP- and VIP-immunopositive neurons or NFH-ir neuronal processes of adult rats. GFAP-immunostaining of large astrocytic processes only occasionally co-localized with GAT1 or GAT3.

Immuno-gold electron microscopic studies of GAT1 and GAT3 localization in SCN

To better describe the location of GAT1 and GAT3, immunogold electron microscopy (EM) was performed. SCN neurons were characterized by deeply invaginated nuclear membranes and somata with well-developed cytoplasmic organelles including the endoplasmic reticulum, Golgi complex, mitochondria and polysomes (Ueda & Ibata, 1989). Immunogold labeling for GAT1 (Fig. 7A) or GAT3 (Fig. 7C) was observed in glial processes, which ensheathed the unlabeled neuronal perikarya. Glial processes were identified in accordance with morphological criteria for recognizing protoplasmic astrocytes (Tamada *et al.*, 1998; Ibata *et al.*, 1999; Kimelberg, 2010). The glial processes containing immunogold labeling could be seen on high-resolution EM images (Fig. 7B, D). GAT1- and GAT3-immunogold labeled glial processes were closely associated with the neuronal cytoplasmic membrane. GAT1-labeled glial processes partially engulfed unlabeled axon terminals and dendrites (Fig. 8A). Glial processes containing immunogold labeling for GAT3 also surrounded unlabeled axon terminals and dendrites that formed symmetric and asymmetric axo-dendritic synapses (Fig. 8B, C). Some of these terminals contained both small clear vesicles,

as well as dense core vesicles, which is typical for axon terminals releasing peptides along with neurotransmitter (Fig. 8C). Fine glial leaflets containing silver-enhanced gold particles enveloped axon terminals (Fig. 8C). Unlabeled dendrites were also partially surrounded by GAT3-ir glial processes. GAT1-ir glial processes enveloped axon bundles that included unmyelinated axons and axonal processes containing clear and dense core vesicles (Fig. 9A). Also, immunogold particles were closely associated with the membranes of GAT3-ir glial processes surrounding unmyelinated axons (Fig. 9B).

Cultured SCN glial cells can express GAT1 and GAT3

To determine if GATs can localize, astrocyte-neuronal cultures were prepared from the SCN. GFAP-immunopositive astrocytes expressed GAT1 (Fig. 10A - C) and GAT3 (Fig. 10D - F). Double staining with antibodies to GAT1 and GAT3 revealed glial cells (presumably astrocytes) immunoreactive to both GATs (Fig. 10G - I). These data demonstrate that an individual glial cell can express both GATs. A model that shows the cell-specific glial localization of GATs in the SCN is presented in Figure 11. This model schematically shows the expression of GABA transporters on the distal processes of GFAP-positive astrocytes and also assumes expression of GATs by GFAP-negative glial cells. The model shows that GAT-ir processes of glial cells surround neuronal cell bodies and axo-dendritic synapses.

DISCUSSION

Our studies confirmed that expression of GAT1 and GAT3 varies in different brain regions. The strongest GAT1 expression was noted in the cerebral cortex exceeding more than twice the expression in the SCN, while GAT3 expression in SCN was 7 times higher than in the cerebral cortex. GAT1 and GAT3 immunogold labeling was observed in fine glial processes surrounding unlabeled neuronal perikarya and axons. Glial processes immunoreactive for GAT3 also partially enveloped unlabeled dendrites and axon terminals that formed symmetric and asymmetric axo-dendritic synapses. Neither GAT1 nor GAT3 immunogold labeling was found in the synaptic cleft indicating that GABA is taken up by transporters in glial processes after its diffusion from the synaptic cleft. The localization and morphology of glial cells immunoreactive for GATs were similar to GFAP-ir protoplasmic astrocytes, described previously in the SCN (Tamada *et al.*, 1998; Ibata *et al.*, 1999; Bushong *et al.*, 2002; Kimelberg, 2010). GAT1 or GAT3 immunoreactivity was also observed in GFAP-immunopositive astrocytes grown in cell cultures. Individual glial cells expressed both GAT1 and GAT3. GATs were not found in SCN neurons identified using a variety of neuronal markers. Perikarya of AVP- or VIP-ir neurons, as well as neuronal processes-ir for Neurofilament Heavy chain, were not immunoreactive for GAT1 or GAT3. Thus, in the SCN of adult rats, like in the other hypothalamic nuclei and thalamus, GAT immunoreactivity was localized in glia while no GAT staining was detected in neurons (De Biasi *et al.*, 1998; Vitellaro-Zuccarello *et al.*, 2003; Park *et al.*, 2009).

In the cerebral cortex and the thalamus during the first two postnatal weeks GATs are expressed in the astrocytic cell bodies, but in adult rats they are localized to the fine distal astrocytic processes that lack intermediate filaments (Vitellaro-Zuccarello *et al.*, 2003).

However, the immunolabeled GFAP cytoskeleton represents only approximately 15% of the total astrocytic volume and includes the soma, primary, and secondary processes, with very little GFAP found in the spongiform processes (Bushong *et al.*, 2002). These fine processes of astrocytes and radial glia-derived cells are too thin to be identified without gold or silver stains (Hajos & Basco, 1984; Morin *et al.*, 1989). This may explain why in the immunofluorescent images of the SCN, large GFAP-positive astrocytic processes did not show significant immunoreactivity for GATs. Also, the tissue stained for GATs often did not contain GFAP-positive astrocytes. In contrast to GFAP-labeled astrocytes, that localized mainly in the ventrolateral part of the SCN (Morin *et al.*, 1989; Tamada *et al.*, 1998; Munekawa *et al.*, 2000; Ikeda *et al.*, 2003; Becquet *et al.*, 2008; Deng *et al.*, 2010), GAT1- and GAT3-immunostaining was relatively even throughout the SCN, suggesting that GFAP-negative glial cells may also express GATs. GFAP-negative glial cells may represent a large part of all glial cells. For example, in the hippocampus GFAP-negative astrocytes represented about 40% of all glial cells (Walz & Lang, 1998). Given that the astroglia to neuron ratio in the SCN is 1 to 3, and each glial cell can enwrap on average four neuronal somata (Guldner, 1983; Halassa *et al.*, 2007b) we conclude that astrocytes expressing GAT1 and GAT3 can regulate the extracellular GABA concentration around a small neuronal population. These functional areas of glial cells influence may play an important role in regulating the activity of the SCN neural network.

Our findings fit well with the concept of a “tripartite” synapse consisting of presynaptic axon terminals, postsynaptic membranes, and astrocytes (Araque *et al.*, 1999; Halassa *et al.*, 2007a). This model helps to explain how glial cells regulate neurotransmission in the SCN by taking up GABA and releasing “gliotransmitters”, which can modulate functional islands of synapses confined within the boundaries of an individual astrocyte (Halassa *et al.*, 2007a). Gliotransmitters are neuroactive substances released from glial cells that act on receptors to alter the activity of neighboring neurons, glial cells or blood vessels, and include glutamate, GABA, ATP, cytokines, and D-serine (Yoon & Lee, 2014; Fields *et al.*, 2015). This concept could be supplemented by astrocyte-mediated GABA uptake from the neuronal somatic membrane. Ensheathment of synapses, neuronal cell bodies and processes by GAT-ir neuroglia would limit GABA spillover and diffusion, regulate the extracellular GABA concentration, and modulate tonic and synaptic GABA currents in the SCN.

Neither GAT1 nor GAT3 expression, as measured by Western blot analysis, showed a diurnal rhythm However, the surface/cytoplasmic expression of GATs in the axonal terminals is dynamic (Deken *et al.*, 2003). For example, about 60% of GAT1 is located on the surface membrane and ~40% in the cytoplasm of presynaptic boutons in mice (Chiu *et al.*, 2002). Therefore, we predict that the proportion of surface versus cytoplasmic GAT in SCN astrocytes may also change during a 24 hour light-dark cycle. In contrast to the pattern of GAT3 expression, GABA and GAD65 mRNA levels in hypothalamus, and particularly in the SCN, peak during lights-on period (Cattabeni *et al.*, 1978; Huhman *et al.*, 1996). In the ventrolateral SCN $GABA_B$ receptor-mediated inhibition of glutamate release from retinohypothalamic tract axon terminals also increased during subjective day (Moldavan & Allen, 2013). The frequency of sIPSCs was increased during the late day and early night in the mouse dorsal SCN (Itri *et al.*, 2004). The ambient GABA level could be regulated by

synaptic or astrocytic GABA release, by change of the surface/cytoplasmic membrane ratio of GATs expression in astrocytes, and/or by functional changes of GATs activity (Chiu *et al.*, 2002; Itri *et al.*, 2004; Yoon & Lee, 2014). These diurnal GABA changes could modulate photic- and non-photic stimuli-induced behavioral shifts. During early and late subjective night, activation of extrasynaptic $GABA_A$ receptors inhibited or abolished the light-induced phase delays (Ehlen & Paul, 2009). In contrast, the inhibition of $GABA_A$ receptors in the SCN increases the magnitude of light-induced phase delays but has no effect on light-induced phase advances (Ralph & Menaker, 1985; Gillespie *et al.*, 1996). It is interesting that the sustained activation of SCN $GABA_A$ receptors induced phase delays of the circadian clock and induced Per expression (Ehlen *et al.*, 2006; Hummer *et al.*, 2015). The activation of $GABA_B$ receptors also reduced the phase-advancing and phase-delaying effects of light during subjective night (Ralph & Menaker, 1989; Gillespie *et al.*, 1997).

It is still not clear how expressed GATs are associated with astrocyte rearrangement in the SCN. Astrocytes express the circadian clock genes Per1 and Per2 and modulation of their activity can alter the timing of the circadian clock (Bennett & Schwartz, 1994; Castel *et al.*, 1997; Jackson, 2011; Ng *et al.*, 2011; Duhart *et al.*, 2013). Circadian rhythmicity was also found in cultures of cortical astrocytes, where the rat Per1::Luc and mouse Per2::Luc astroglia expressed circadian rhythms with a genetically determined period (Prolo *et al.*, 2005; Beaule *et al.*, 2009). Data about diurnal GFAP expression in the SCN are controversial. GFAP immunoreactivity was not found to oscillate in the SCN of rats during the LD cycle (Tamada *et al.*, 1998). Other studies showed that the environmental light and dark phases regulate GFAP expression in SCN astrocytes and their coverage of the soma and dendrites of VIP- and AVP-expressing SCN neurons (Becquet *et al.*, 2008; Girardet *et al.*, 2010a; Girardet *et al.*, 2010b). The retraction and extension of astrocytic processes could alter the activity of both inhibitory and excitatory synapses. Also, seasonal diurnal changes of GFAP expression were found in rat SCN. In the winter, GFAP expression was low during the day and high at night while in the summer an opposite expression pattern was observed. The changes of GFAP expression were interpreted as a hypertrophy of pre-existing astrocytes due to alternating photic stimulation (Gerics *et al.*, 2006). The peak of circadian GFAP expression in the ventrolateral rat SCN, which is the main recipient of retinal afferents, was observed at ZT18 (Becquet *et al.*, 2008). The misalignment between the GABA transporters and GFAP expression requires further investigation.

Our studies demonstrated that GAT1 and GAT3 were expressed in glial cells but not at detectable levels in SCN neurons. Thus, glial cells expressing GAT1 and GAT3 may regulate the GABA concentration in synaptic and extrasynaptic compartments of SCN, as well as fast and tonic GABA neurotransmission.

Acknowledgements

The work was supported by National Institutes of Health (NIH) grants R01 NS036607 to CNA and P30 NS061800 to SAA. The authors wish to thank Dr. Karin Mullendorff and Dr. Linda Ruggiero for advice on Western blotting and immunohistochemistry techniques, and Sam Hermes for immunogold tissue processing. We would like to thank Dr. Michael Hughes for helpful advice in analyzing our data with JTK_Cycle. For technical assistance, we acknowledge Dr. Stefanie Kaech Petrie and Aurelie Snyder, of the Advanced Light Microscopy Core (ALM) at The Jungers Center (OHSU), which is supported by shared instrumentation grants S10 RR023432 and S10 RR025440

from the National Center for Research Resources (NIH). The electron microscope was purchased through an instrumentation grant from Murdock Charitable Trust (TEM).

Abbreviations

ACSF	artificial cerebrospinal fluid
BSA	bovine serum albumin
$GABA_ARs$	$GABA_A$ receptors
GAT1	GABA transporter 1
GAT3	GABA transporter 3
GATs	GABA transporters
LD cycle	light-dark cycle
SCN	suprachiasmatic nucleus
RHT	retinohypothalamic tract
WB	Western blot
IHC	immunohistochemistry
EM	electron microscopy
ir	immunoreactive
ZT	Zeitgeber time
3V	third ventricle
Och	optic chiasm

References

Aguilar-Roblero R, Verduzco-Carbajal L, Rodríguez C, Mendez-Franco J, Morán J, Perez de la Mora M. Circadian rhythmicity in the GABAergic system in the suprachiasmatic nuclei of the rat. Neurosci. Lett. 1993; 157:199–202. [PubMed: 8233053]

Aicher SA, Mitchell JL, Swanson KC, Zadina JE. Endomorphin-2 axon terminals contact mu-opioid receptor-containing dendrites in trigeminal dorsal horn. Brain. Res. 2003a; 977:190–198. [PubMed: 12834879]

Aicher SA, Sharma S, Mitchell JL. Structural changes in AMPA-receptive neurons in the nucleus of the solitary tract of spontaneously hypertensive rats. Hypertension. 2003b; 41:1246–1252. [PubMed: 12695422]

Albus H, Vansteensel MJ, Michel S, Block GD, Meijer JH. A GABAergic mechanism is necessary for coupling dissociable ventral and dorsal regional oscillators within the circadian clock. Curr. Biol. 2005; 15:886–893. [PubMed: 15916945]

Araque A, Parpura V, Sanzgiri RP, Haydon PG. Tripartite synapses: glia, the unacknowledged partner. Trends Neurosci. 1999; 22:208–215. [PubMed: 10322493]

Aton SJ, Huettner JE, Straume M, Herzog ED. GABA and Gi/o differentially control circadian rhythms and synchrony in clock neurons. P. Natl. Acad. Sci. USA. 2006; 103:19188–19193.

Beaule C, Swanstrom A, Leone MJ, Herzog ED. Circadian modulation of gene expression, but not glutamate uptake, in mouse and rat cortical astrocytes. PLoS ONE. 2009; 4:e7476. [PubMed: 19829696]

Becquet D, Girardet C, Guillaumond F, Francois-Bellan AM, Bosler O. Ultrastructural plasticity in the rat suprachiasmatic nucleus. Possible involvement in clock entrainment. Glia. 2008; 56:294–305. [PubMed: 18080293]

Belenky MA, Yarom Y, Pickard GE. Heterogeneous expression of gamma-aminobutyric acid and gamma-aminobutyric acid-associated receptors and transporters in the rat suprachiasmatic nucleus. J. Comp. Neurol. 2008; 506:708–732. [PubMed: 18067149]

Bennett MR, Schwartz WJ. Are glia among the cells that express immunoreactive c-Fos in the suprachiasmatic nucleus? Neuroreport. 1994; 5:1737–1740. [PubMed: 7827320]

Borden LA. GABA transporter heterogeneity: pharmacology and cellular localization. Neurochem. Int. 1996; 29:335–356. [PubMed: 8939442]

Bushong EA, Martone ME, Jones YZ, Ellisman MH. Protoplasmic astrocytes in CA1 stratum radiatum occupy separate anatomical domains. J. Neurosci. 2002; 22:183–192. [PubMed: 11756501]

Cardinali DP, Golombek DA. The rhythmic GABAergic system. Neurochem. Res. 1998; 23:607–614. [PubMed: 9566598]

Castel M, Belenky M, Cohen S, Wagner S, Schwartz WJ. Light-induced c-Fos expression in the mouse suprachiasmatic nucleus: immunoelectron microscopy reveals co-localization in multiple cell types. Eur. J. Neurosci. 1997; 9:1950–1960. [PubMed: 9383218]

Cattabeni F, Maggi A, Monduzzi M, De Angelis L, Racagni G. GABA: circadian fluctuations in rat hypothalamus. J. Neurochem. 1978; 31:565–5667. [PubMed: 671058]

Chiu CS, Jensen K, Sokolova I, Wang D, Li M, Deshpande P, Davidson N, Mody I, Quick MW, Quake SR, Lester HA. Number, density, and surface/cytoplasmic distribution of GABA transporters at presynaptic structures of knock-in mice carrying GABA transporter subtype 1-green fluorescent protein fusions. J. Neurosci. 2002; 22:10251–10266. [PubMed: 12451126]

De Biasi S, Vitellaro-Zuccarello L, Brecha NC. Immunoreactivity for the GABA transporter-1 and GABA transporter-3 is restricted to astrocytes in the rat thalamus. A light and electron-microscopic immunolocalization. Neuroscience. 1998; 83:815–828. [PubMed: 9483565]

De Jeu M, Pennartz CMA. Circadian modulation of GABA function in the rat suprachiasmatic nucleus: excitatory effects during the night phase. J. Neurophysiol. 2002; 87:834–844. [PubMed: 11826050]

Deken SL, Wang D, Quick MW. Plasma membrane GABA transporters reside on distinct vesicles and undergo rapid regulated recycling. J. Neurosci. 2003; 23:1563–1568. [PubMed: 12629157]

Deng XH, Bertini G, Palomba M, Xu YZ, Bonaconsa M, Nygard M, Bentivoglio M. Glial transcripts and immune-challenged glia in the suprachiasmatic nucleus of young and aged mice. Chronobiol. Int. 2010; 27:742–767. [PubMed: 20560709]

Duhart JM, Leone MJ, Paladino N, Evans JA, Castanon-Cervantes O, Davidson AJ, Golombek DA. Suprachiasmatic astrocytes modulate the circadian clock in response to TNF-alpha. J. Immunol. 2013; 191:4656–4664. [PubMed: 24062487]

Ehlen JC, Novak CM, Karom MC, Gamble KL, Paul KN, Albers HE. GABAA receptor activation suppresses Period 1 mRNA and Period 2 mRNA in the suprachiasmatic nucleus during the mid-subjective day. Eur. J. Neurosci. 2006; 23:3328–3336. [PubMed: 16820022]

Ehlen JC, Paul KN. Regulation of light's action in the mammalian circadian clock: role of the extrasynaptic GABAA receptor. Am. J. Physiol. - Reg. I. 2009; 296:R1606–1612.

Fields RD, Woo DH, Basser PJ. Glial Regulation of the Neuronal Connectome through Local and Long-Distant Communication. Neuron. 2015; 86:374–386. [PubMed: 25905811]

Gerics B, Szalay F, Hajos F. Glial fibrillary acidic protein immunoreactivity in the rat suprachiasmatic nucleus: circadian changes and their seasonal dependence. J. Anat. 2006; 209:231–237. [PubMed: 16879601]

Gillespie CF, Huhman KL, Babagbemi TO, Albers HE. Bicuculline increases and muscimol reduces the phase-delaying effects of light and VIP/PHI/GRP in the suprachiasmatic region. J. Biol. Rhythm. 1996; 11:137–144.

Gillespie CF, Mintz EM, Marvel CL, Huhman KL, Albers HE. GABAA and GABAB agonists and antagonists alter the phase-shifting effects of light when microinjected into the suprachiasmatic region. Brain Res. 1997; 759:181–189. [PubMed: 9221935]

Gillette MU. The suprachiasmatic nuclei: circadian phase-shifts induced at the time of hypothalamic slice preparation are preserved in vitro. Brain Res. 1986; 379:176–181. [PubMed: 3742212]

Girardet C, Becquet D, Blanchard MP, Francois-Bellan AM, Bosler O. Neuroglial and synaptic rearrangements associated with photic entrainment of the circadian clock in the suprachiasmatic nucleus. Eur. J. Neurosci. 2010a; 32:2133–2142. [PubMed: 21143667]

Girardet C, Blanchard MP, Ferracci G, Leveque C, Moreno M, Francois-Bellan AM, Becquet D, Bosler O. Daily changes in synaptic innervation of VIP neurons in the rat suprachiasmatic nucleus: contribution of glutamatergic afferents. Eur J. Neurosci. 2010b; 31:359–370. [PubMed: 20074215]

Gompf HS, Allen CN. GABAergic synapses of the suprachiasmatic nucleus exhibit a diurnal rhythm of short-term synaptic plasticity. Eur. J.Neurosci. 2004; 19:2791–2798. [PubMed: 15147312]

Green DJ, Gillette R. Circadian rhythm of firing rate recorded from single cells in the rat suprachiasmatic brain slice. Brain Res. 1982; 245:198–200. [PubMed: 6889453]

Groos GA, Hendriks J. Circadian rhythms in electrical discharge of rat suprachiasmatic neurones recorded in vitro. Neurosci. Lett. 1982; 34:283–288. [PubMed: 6298675]

Guldner FH. Numbers of neurons and astroglial cells in the suprachiasmatic nucleus of male and female rats. Exp. Brain Res. 1983; 50:373–376. [PubMed: 6641871]

Hajos F, Basco E. The surface-contact glia. Adv. Anat. Embryol. Cel. 1984; 84:1–79.

Halassa MM, Fellin T, Haydon PG. The tripartite synapse: roles for gliotransmission in health and disease. Trends Molecul. Med. 2007a; 13:54–63.

Halassa MM, Fellin T, Takano H, Dong JH, Haydon PG. Synaptic islands defined by the territory of a single astrocyte. J. Neurosci. 2007b; 27:6473–6477. [PubMed: 17567808]

Huettner JE, Baughman RW. Primary culture of identified neurons from the visual cortex of postnatal rats. J. Neurosci. 1986; 6:3044–3060. [PubMed: 3760948]

Huhman KL, Hennessey AC, Albers HE. Rhythms of glutamic acid decarboxylase mRNA in the suprachiasmatic nucleus. J. Biol. Rhythm. 1996; 11:311–316.

Hughes ME, Hogenesch JB, Kornacker K. JTK_CYCLE: an efficient nonparametric algorithm for detecting rhythmic components in genome-scale data sets. J. Biol Rhythm. 2010; 25:372–380.

Hummer DL, Ehlen JC, Larkin TE 2nd, McNeill J.K.t. Pamplin JR 2nd, Walker CA, Walker PV 2nd, Dhanraj DR, Albers HE. Sustained activation of GABAA receptors in the suprachiasmatic nucleus mediates light-induced phase delays of the circadian clock: a novel function of ionotropic receptors. Eur. J. Neurosci. 2015; 42:1830–1838. [PubMed: 25865743]

Ibata Y, Okamura H, Tanaka M, Tamada Y, Hayashi S, Iijima N, Matsuda T, Munekawa K, Takamatsu T, Hisa Y, Shigeyoshi Y, Amaya F. Functional morphology of the suprachiasmatic nucleus. Front. Neuroendocrinol. 1999; 20:241–268. [PubMed: 10433864]

Ikeda T, Iijima N, Munekawa K, Ishihara A, Ibata Y, Tanaka M. Functional retinal input stimulates expression of astroglial elements in the suprachiasmatic nucleus of postnatal developing rat. Neurosci. Res. 2003; 47:39–45. [PubMed: 12941445]

Ikegaki N, Saito N, Hashima M, Tanaka C. Production of specific antibodies against GABA transporter subtypes (GAT1, GAT2, GAT3) and their application to immunocytochemistry. Mol. Brain Res. 1994; 26:47–54. [PubMed: 7854065]

Isobe Y, Nishino H. GABAergic control of Arg-vasopressin release from suprachiasmatic nucleus slice culture. Brain Res. 1997; 755:213–220. [PubMed: 9175889]

Itouji A, Sakai N, Tanaka C, Saito N. Neuronal and glial localization of two GABA transporters (GAT1 and GAT3) in the rat cerebellum. Mol. Brain Res. 1996; 37:309–316. [PubMed: 8738166]

Itri J, Michel S, Waschek JA, Colwell CS. Circadian rhythm in inhibitory synaptic transmission in the mouse suprachiasmatic nucleus. J. Neurophysiol. 2004; 92:311–319. [PubMed: 14973316]

Jackson FR. Glial cell modulation of circadian rhythms. Glia. 2011; 59:1341–1350. [PubMed: 21732426]

Jin XT, Galvan A, Wichmann T, Smith Y. Localization and Function of GABA Transporters GAT-1 and GAT-3 in the Basal Ganglia. Front. System. Neurosci. 2011; 5:63.

Kaech S, Banker G. Culturing hippocampal neurons. Nat. Protoc. 2006; 1:2406–2415. [PubMed: 17406484]

Kimelberg HK. Functions of mature mammalian astrocytes: a current view. Neuroscientist. 2010; 16:79–106. [PubMed: 20236950]

Lelong IH, Petegnief V, Rebel G. Neuronal cells mature faster on polyethyleneimine coated plates than on polylysine coated plates. J. Neurosci. Res. 1992; 32:562–568. [PubMed: 1527802]

Luquin E, Perez-Lorenzo E, Aymerich MS, Mengual E. Two-color fluorescence labeling in acrolein-fixed brain tissue. J. Histochem. Cytochem. 2010; 58:359–368. [PubMed: 20051381]

Madsen KK, White HS, Schousboe A. Neuronal and non-neuronal GABA transporters as targets for antiepileptic drugs. Pharmacol. Therapeut. 2010; 125:394–401.

Mathews PJ, Lee KH, Peng Z, Houser CR, Otis TS. Effects of climbing fiber driven inhibition on Purkinje neuron spiking. J. Neurosci. 2012; 32:17988–17997. [PubMed: 23238715]

Minelli A, Brecha NC, Karschin C, DeBiasi S, Conti F. GAT-1, a high-affinity GABA plasma membrane transporter, is localized to neurons and astroglia in the cerebral cortex. J. Neurosci. 1995; 15:7734–7746. [PubMed: 7472524]

Minelli A, DeBiasi S, Brecha NC, Zuccarello LV, Conti F. GAT-3, a high-affinity GABA plasma membrane transporter, is localized to astrocytic processes, and it is not confined to the vicinity of GABAergic synapses in the cerebral cortex. J. Neurosci. 1996; 16:6255–6264. [PubMed: 8815906]

Moldavan MG, Allen CN. GABAB receptor-mediated frequency-dependent and circadian changes in synaptic plasticity modulate retinal input to the suprachiasmatic nucleus. J. Physiol. 2013; 591:2475–2490. [PubMed: 23401614]

Moore RY, Speh JC. GABA is the principal neurotransmitter of the circadian system. Neurosci. Lett. 1993; 150:112–116. [PubMed: 8097023]

Morin LP, Johnson RF, Moore RY. Two brain nuclei controlling circadian rhythms are identified by GFAP immunoreactivity in hamsters and rats. Neurosci. Lett. 1989; 99:55–60. [PubMed: 2664580]

Munekawa K, Tamada Y, Iijima N, Hayashi S, Ishihara A, Inoue K, Tanaka M, Ibata Y. Development of astroglial elements in the suprachiasmatic nucleus of the rat: with special reference for the involvement of the optic nerve. Exp. Neurol. 2000; 166:44–51. [PubMed: 11031082]

Ng FS, Tangredi MM, Jackson FR. Glial cells physiologically modulate clock neurons and circadian behavior in a calcium-dependent manner. Curr. Biol. 2011; 21:625–634. [PubMed: 21497088]

Park JB, Jo JY, Zheng H, Patel KP, Stern JE. Regulation of tonic GABA inhibitory function, presympathetic neuronal activity and sympathetic outflow from the paraventricular nucleus by astroglial GABA transporters. J. Physiol. 2009; 587:4645–4660. [PubMed: 19703969]

Prolo LM, Takahashi JS, Herzog ED. Circadian rhythm generation and entrainment in astrocytes. J. Neurosci. 2005; 25:404–408. [PubMed: 15647483]

Ralph MR, Menaker M. Bicuculline blocks circadian phase delays but not advances. Brain Res. 1985; 325:362–365. [PubMed: 3978427]

Ralph MR, Menaker M. GABA regulation of circadian responses to light. I. Involvement of GABAA-benzodiazepine and GABAB receptors. J. Neurosci. 1989; 9:2858–2865. [PubMed: 2549220]

Ren D, Miller JD. Primary cell culture of suprachiasmatic nucleus. Brain Res. Bull. 2003; 61:547–553. [PubMed: 13679255]

Ribak CE, Tong WM, Brecha NC. Astrocytic processes compensate for the apparent lack of GABA transporters in the axon terminals of cerebellar Purkinje cells. Anat. Embryol. 1996a; 194:379–390. [PubMed: 8896702]

Ribak CE, Tong WM, Brecha NC. GABA plasma membrane transporters, GAT-1 and GAT-3, display different distributions in the rat hippocampus. J. Comp. Neurol. 1996b; 367:595–606. [PubMed: 8731228]

Scimemi A. Plasticity of GABA transporters: an unconventional route to shape inhibitory synaptic transmission. Front. Cell. Neurosci. 2014; 8:128. [PubMed: 24860430]

Shibata S, Oomura Y, Kita H, Hattori K. Circadian rhythmic changes of neuronal activity in the suprachiasmatic nucleus of the rat hypothalamic slice. Brain Res. 1982; 247:154–158. [PubMed: 7127113]

Tamada Y, Tanaka M, Munekawa K, Hayashi S, Okamura H, Kubo T, Hisa Y, Ibata Y. Neuron-glia interaction in the suprachiasmatic nucleus: A double labeling light and electron microscopic immunocytochemical study in the rat. Experimental Neurol. 1998; 45:281–287.

Ueda S, Ibata Y. The fine structures of the suprachiasmatic nucleus of the golden hamster. J. Hirnforsch. 1989; 30:719–729. [PubMed: 2628491]

vanderLeest HT, Vansteensel MJ, Duindam H, Michel S, Meijer JH. Phase of the electrical activity rhythm in the SCN in vitro not influenced by preparation time. Chronobiol. Int. 2009; 26:1075–1089. [PubMed: 19731107]

Vitellaro-Zuccarello L, Calvaresi N, De Biasi S. Expression of GABA transporters, GAT-1 and GAT-3, in the cerebral cortex and thalamus of the rat during postnatal development. Cell Tissue Res. 2003; 313:245–257. [PubMed: 12898208]

Wagner S, Castel M, Gainer H, Yarom Y. GABA in the mammalian suprachiasmatic nucleus and its role in diurnal rhythmicity. Nature. 1997; 387:598–603. [PubMed: 9177347]

Walz W, Lang MK. Immunocytochemical evidence for a distinct GFAP-negative subpopulation of astrocytes in the adult rat hippocampus. Neurosci. Lett. 1998; 257:127–130. [PubMed: 9870336]

Yoon BE, Lee CJ. GABA as a rising gliotransmitter. Front. Neural. Circuits. 2014; 8:141. [PubMed: 25565970]

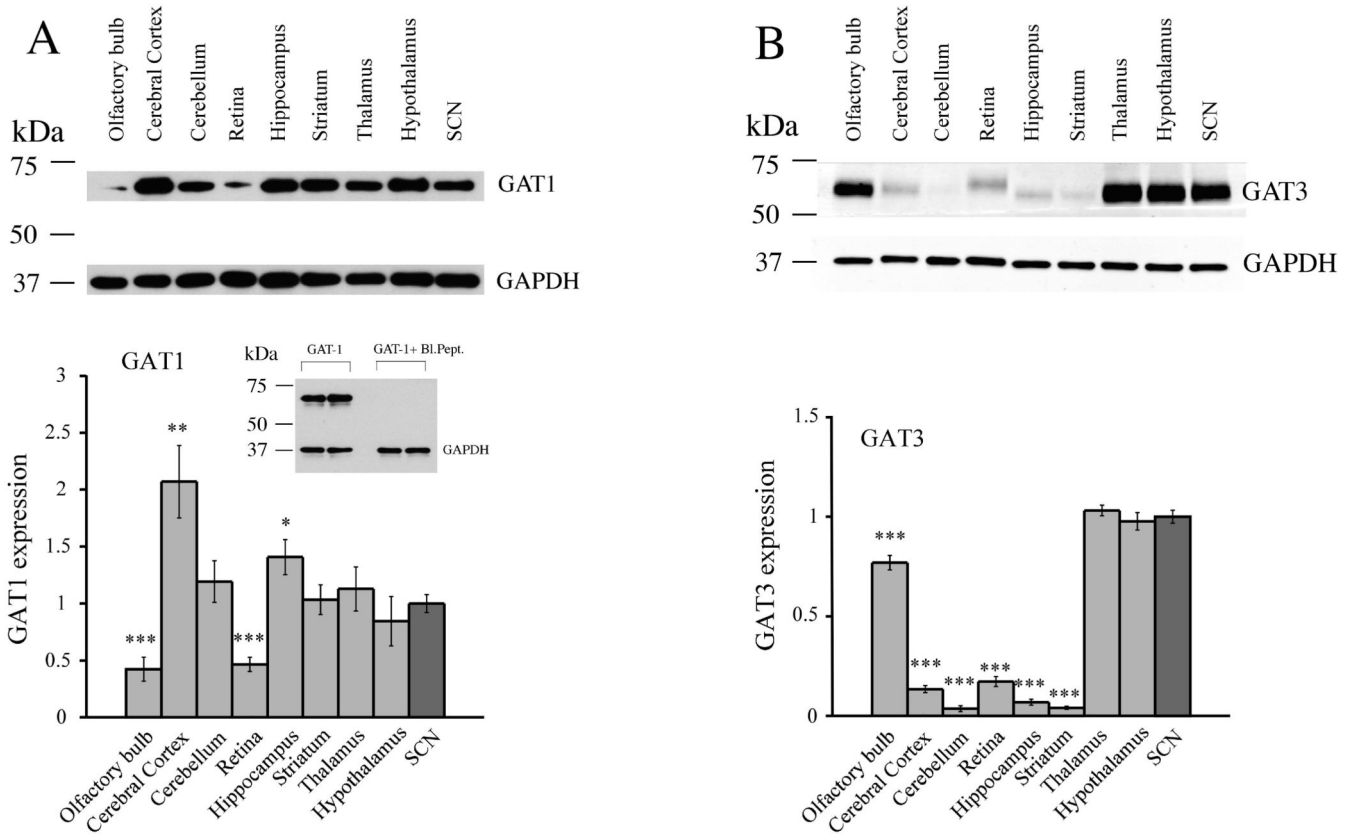

Figure 1. Relative expression levels of GAT1 and GAT3 in other brain regions compared to the SCN

A and B: Western blot and quantitative analysis of GAT1 and GAT3 expression, respectively. *Upper*: immunoblot, GAT bands (*top line*), and the loading control: GAPDH (*bottom line*). Molecular mass markers (kDa) are indicated. *Lower*: optical density (O.D.) was measured and quantified with ImageJ software, then normalized to the loading control (shown in ratio units). Each bar represents the ratio of GAT expression in each brain region to the SCN level. Error bars represent the SEM, * $p < 0.05$, ** $p < 0.01$, *** $p < 0.001$ when compared with SCN. Each histogram represents O.D. measurements from 5 gels (mean ± SE). A. *In insert:* Blocking peptide (Bl. pept., Alomone Labs Ltd.) completely blocked GAT1 detection in the cerebral cortex sample (positive control). Anti-GAT1 antibody alone and anti-GAT1 antibody + blocking peptide (Bl. pept., Alomone Labs) are shown in duplicates. A detailed description of antibodies is in Table 1 and in *Methods*. These data demonstrate that GAT1 is more widely expressed in the brain than GAT3. In contrast to GAT1, the GAT3 expression is more prominent in the thalamus and hypothalamus including the SCN.

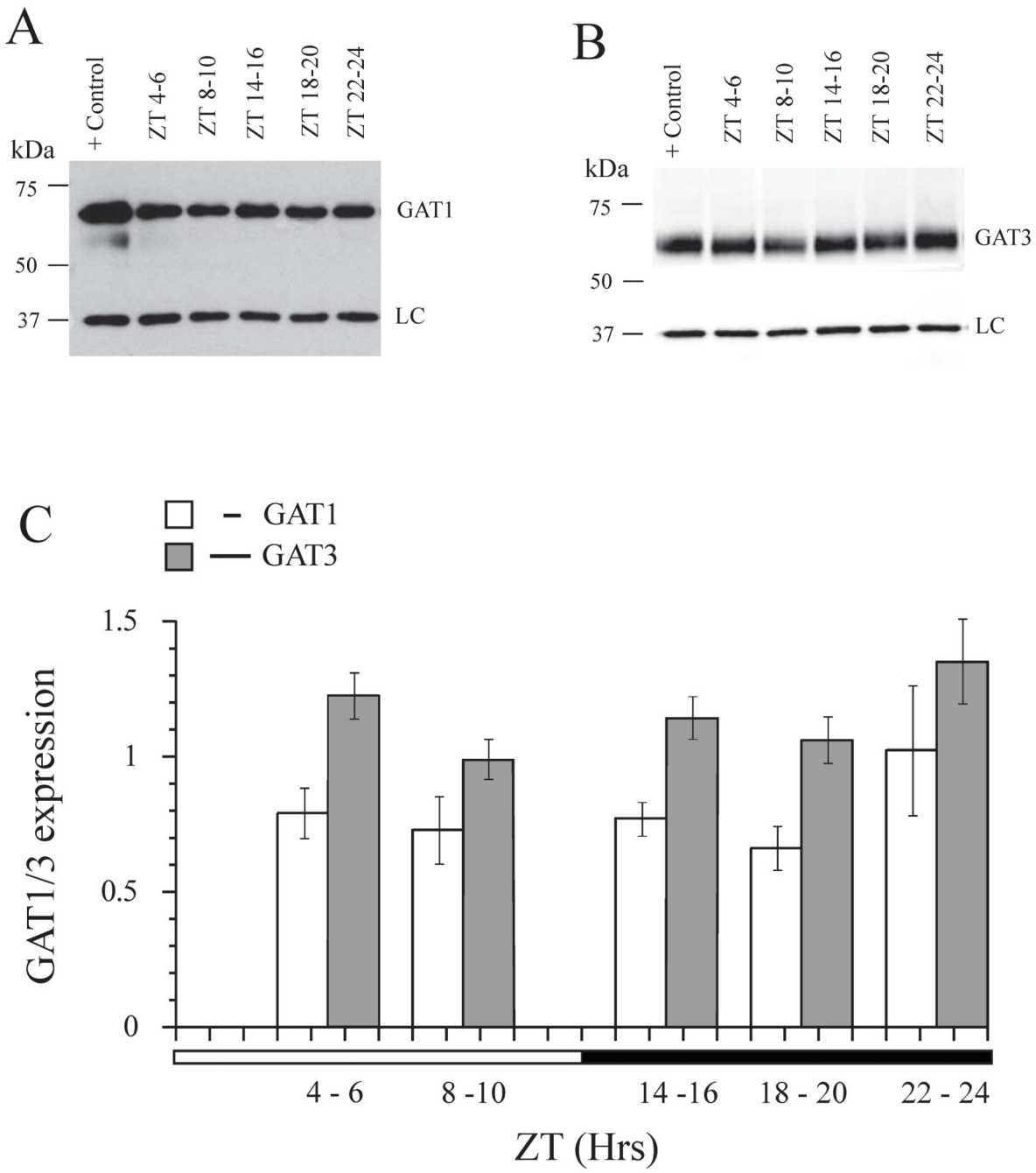

Figure 2. Diurnal expression of GAT3 and GAT1 in the SCN of rats on a 12:12h LD cycle

A. Western blot for GAT1, each band represents one of five zeitgeber times (ZT)s: ZT 4 - 6, ZT 8 - 10; ZT 14 - 16; ZT 18 - 20; ZT 22 - 24. Positive control is the cerebral cortex. Loading control (LC): GAPDH. B. Western blot for GAT3. Positive control is the thalamus. C. Graph shows GAT1 and GAT3 expression at different ZTs. The quantification of the optical density of the bands was performed, than data were normalized to the loading control. GAT1: 4 gels in duplicate i.e. 8 bands for each ZT. GAT3: 5 gels in duplicate i.e.10 bands for each ZT. The light and dark phases of the cycle are shown on the horizontal bar

under the graph. Neither GAT1 nor GAT3 showed a diurnal rhythm of expression. Data shown as mean ± SEM. A detailed description of the antibodies is in Table 1 and in *Method*s. The rest of the notations are the same, as those in Fig.1.

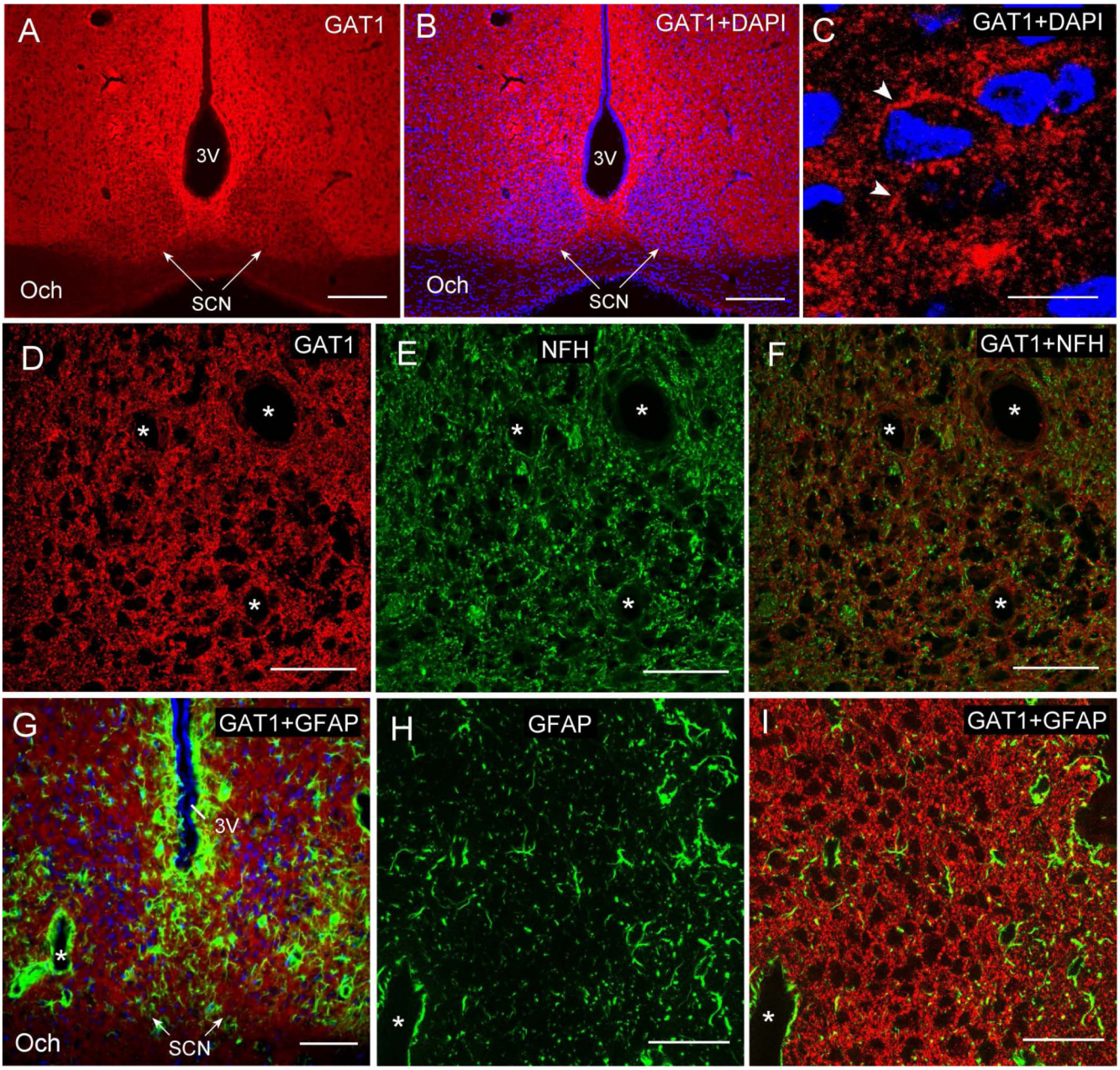

Figure 3. GAT1-immunoreactivity in the SCN

A, B. Coronal section of the hypothalamus including the SCN, demonstrating high levels of GAT1 (red) expression in the region of the periventricular hypothalamic nuclei and the region between the lobes of the SCN. 10×, scale bar 200 μm. The brain was extracted and the tissue fixed at ZT 4 - 5 (A, B) and at ZT 18 - 20 (C – I). C. Higher magnification image showing GAT1-ir punctas surrounding cell bodies in the SCN (arrowheads), 60×, scale bar 10 μm. B and C. Sections were counterstained with DAPI (blue) to show the location of cellular nuclei and to outline the SCN. D - F. GAT1 (D) and NFH (green, E) expression. A merged GAT1 and NFH image is shown in F. Note the lack of overlap between the GAT1 and NFH expression. G. Low magnification image (20×) showing GAT1 and GFAP (green)

expression in the SCN, scale bar 100 μm. H. Higher magnification showing GFAP (green) expression. I. Merged image of GAT1 and GFAP staining. There was only occasional overlap between the two stains. D - F, H, I, 60×, scale bar 50 μm. Rabbit anti-GAT1 antibody (ab72448, Abcam) was used for all images, except for A and B (rabbit anti-GAT1 antibody, AB1570, Millipore). SCN – hypothalamic suprachiasmatic nucleus, 3V – third ventricle, Och - optic chiasm. D – I. Asterisks – blood vessels. Description of antibodies is shown in Table 1.

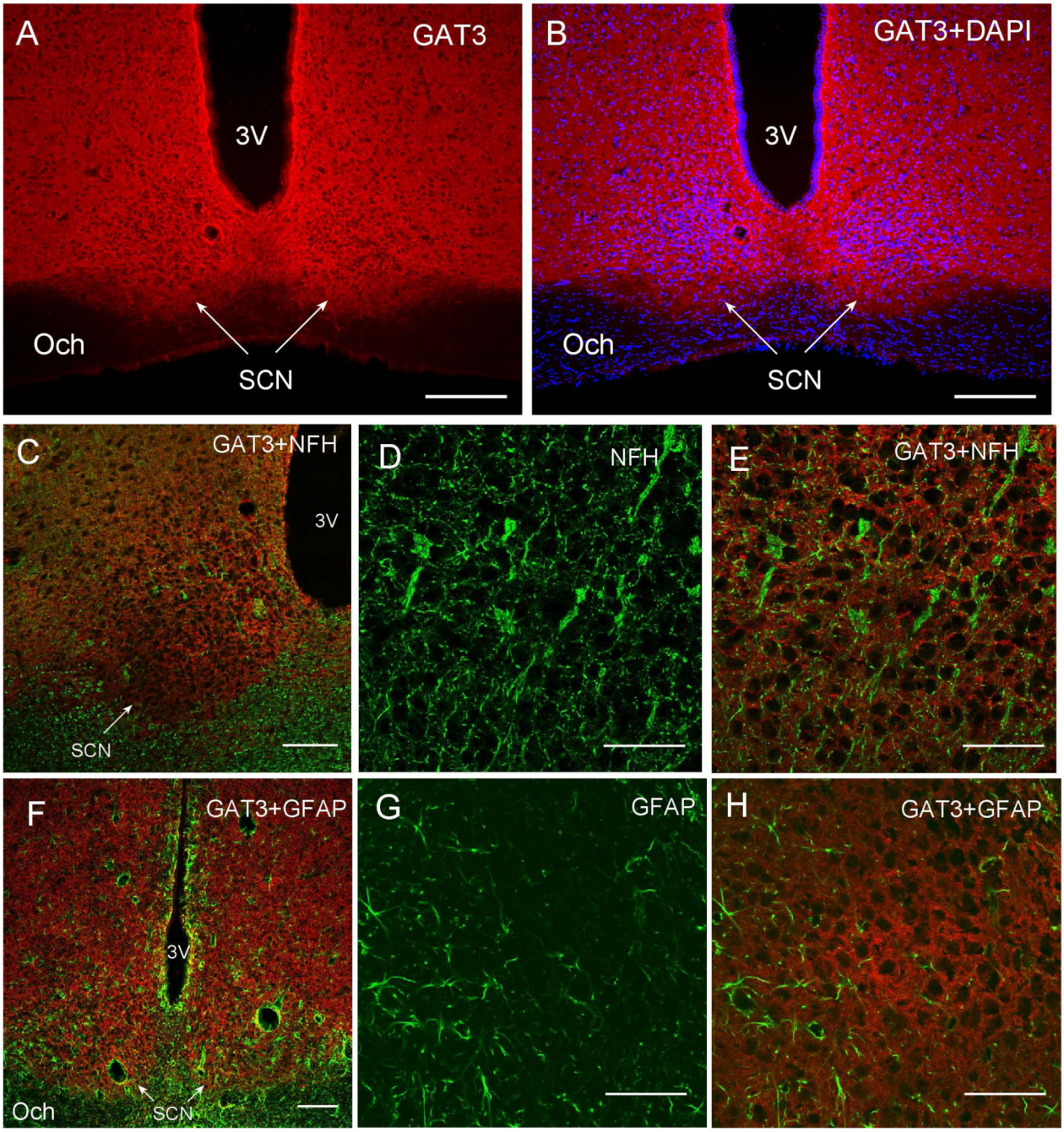

Figure 4. GAT3-immunoreactivity in SCN

A, B. Coronal section of the hypothalamus including the SCN, demonstrating GAT3 (red) expression in hypothalamus and SCN with high level of expression around 3-rd ventricles and in SCNs. 10×, scale bar 200 μm. The brain was extracted and the tissue fixed at ZT 4 - 5 (A, B) and at ZT 18 - 20 (C – H). B. Section counterstained with DAPI (blue) to outline the SCN, 10×, scale bar 200 μm. C. Low magnification (20×) image showing the expression of GAT3 and NFH (green). D. Higher magnification image showing NFH expression. E. Merged image showing GAT3 and NFH expression. Note that the GAT3- and NFH-positive

processes are not co-localized. F. Low magnification image demonstrating GAT3 and GFAP expression (green) in the SCN, 10× G. Higher magnification image of GFAP expression. H. Merged image showing GAT3 and GFAP expression. C, E, F, H, I. Confocal images, 60×. Scale bars 50 μm. D, G. Scale bar 100 μm. Description of antibodies is shown in Table 1. The rest of the notations are the same, as those in Fig. 3.

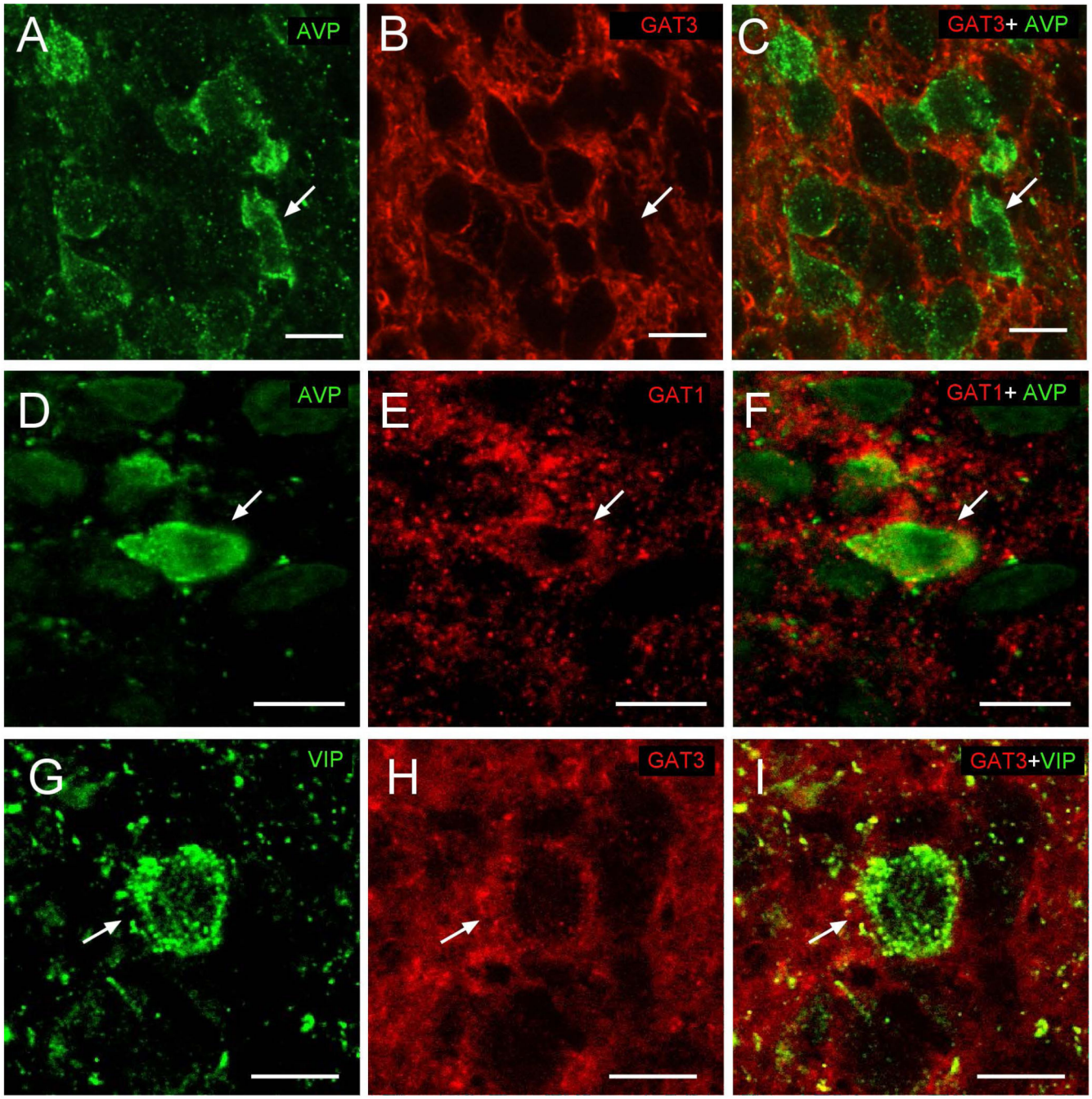

Figure 5. GAT1 and GAT3 were not expressed in neurons immunoreactive for arginine vasopressin (AVP) or vasoactive intestinal peptide (VIP)

A - I. Double-labeling with antibodies to GAT1 or GAT3 and AVP or VIP. A – C. Application of AVP (, green, (A)) and GAT3 (, red (B), merged images (C). D - F. Application of AVP (D) and GAT1 (, red, (E)), merged images (F). G – I. VIP (green, G) and GAT3 (H), merged images (I). Arrows – neurons immunoreactive to AVP or VIP. Note: neurons labeled for AVP or VIP did not show GAT1 or GAT3 expression. All images were taken at 60×, scale bar 10 μm. Rats were perfused for IHC at ZT 18 - 20.

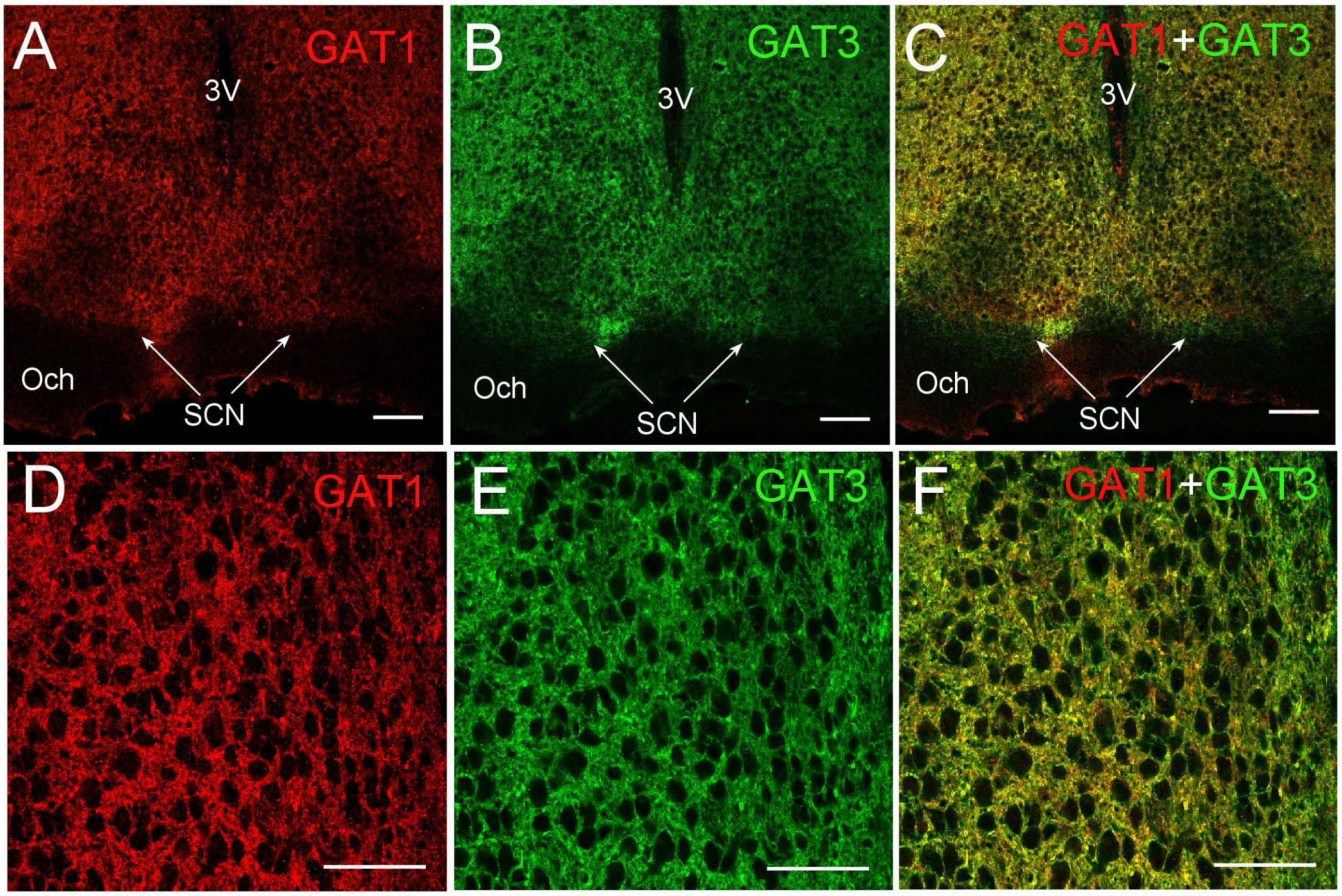

Figure 6. GAT1 and GAT3 are co-localized in the SCN

A - F. Brain sections of adult rats stained for GAT1 (red) and GAT3 (green) showing significant overlap in the expression pattern of these transporters C, F. Merged images. A - C. Low magnification, 10×, scale bar: 100 μm. D - F. Higher magnification, 60×, scale bar: 50 μm. Rats were perfused for IHC at ZT 18 - 20.

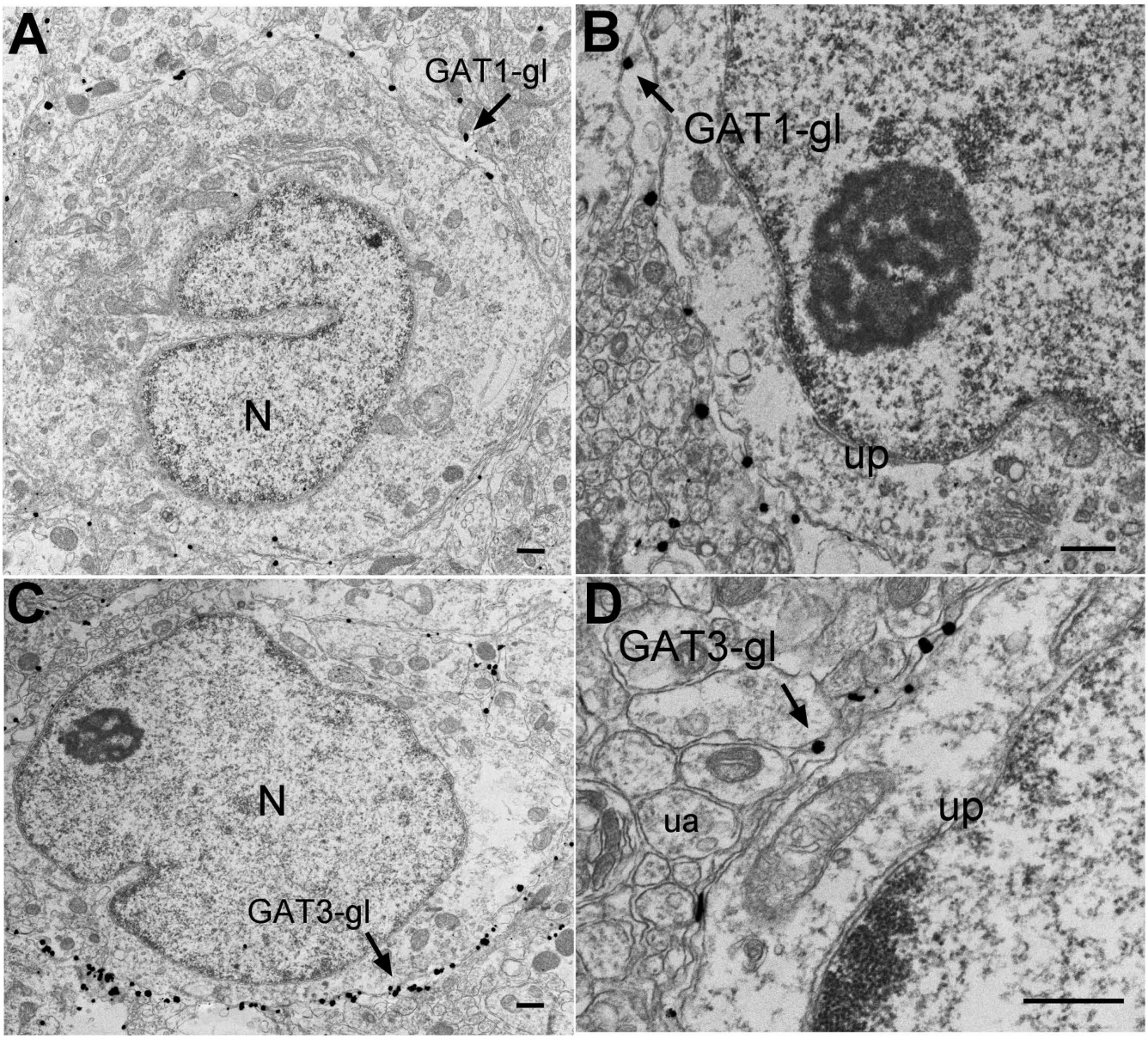

Figure 7. GAT1- and GAT3-immunogold labeling (−IL) in glial processes surrounding perikarya in the SCN

A, B. GAT1- IL, C, D. GAT3-IL. A. An unlabeled cell body is surrounded by glial processes containing IL for GAT1 (arrow, GAT1-gl). B. A high magnification image shows immunogold particles (arrow) associated with glial processes near an unlabeled perikaryon (up). C. IL for GAT3 (arrow, GAT3-gl) is associated with glial processes near an unlabeled cell body. The cell displays a large nucleus (N) and limited cytoplasm. D. A high magnification image shows GAT3-ir glial processes between an unlabeled perikaryon (up) and groups of unmyelinated axons (ua) nearby. The immungold particles (arrow) are closely associated with glial cell membranes. Scale bars 500 nm.

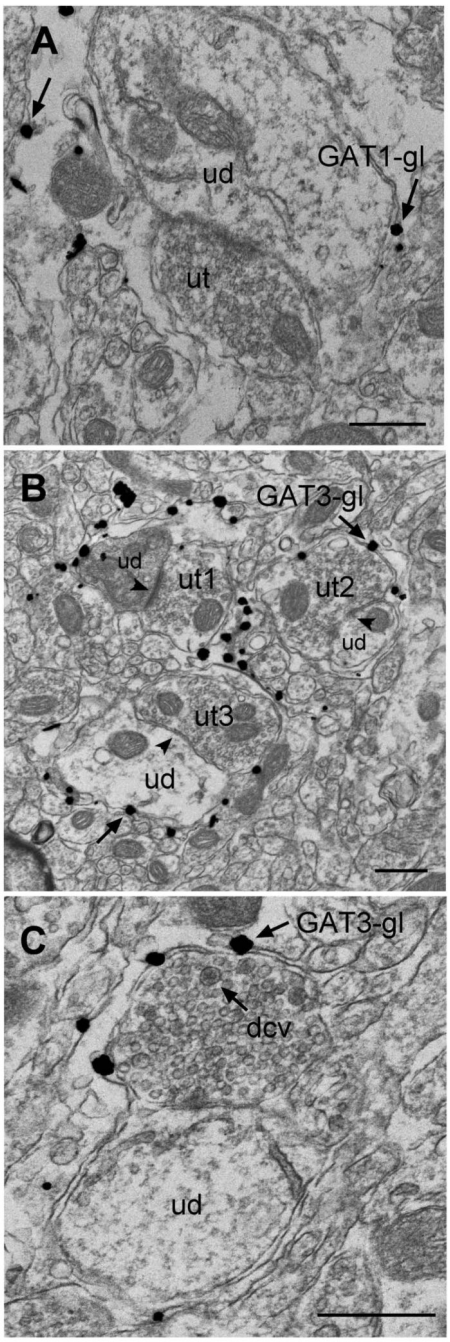

Figure 8. GAT1- and GAT3-ir glial cells are closely associated with synaptic complexes

A. GAT1-immunogold labeled glial processes (arrow, GAT1-gl) surround a synaptic complex that consists of an unlabeled axon terminal (ut) and unlabeled dendrite (ud). B. Three unlabeled axon terminals (ut1 – ut3) form contacts with unlabeled dendrites (ud). One axon terminal (ut1) forms an asymmetric synapse (arrow head) with a dendrite, while nearby another axon terminal (ut3) forms a symmetric synapse (arrow head) with a dendrite. The third terminal (ut2) is apposed to an unlabeled dendrite without a clear synaptic junction. All three dendritic complexes are ensheathed in GAT3-ir glial processes (arrows, GAT3-gl)

indicated by immungold particles. C. A GAT3-ir glial process (arrow) is apposed to an axon terminal that contains both small clear vesicles, as well as dense core vesicles (dcv). An unlabeled dendrite (ud) is also partially surrounded by GAT3-ir glial processes. Scale bars: 500 nm.

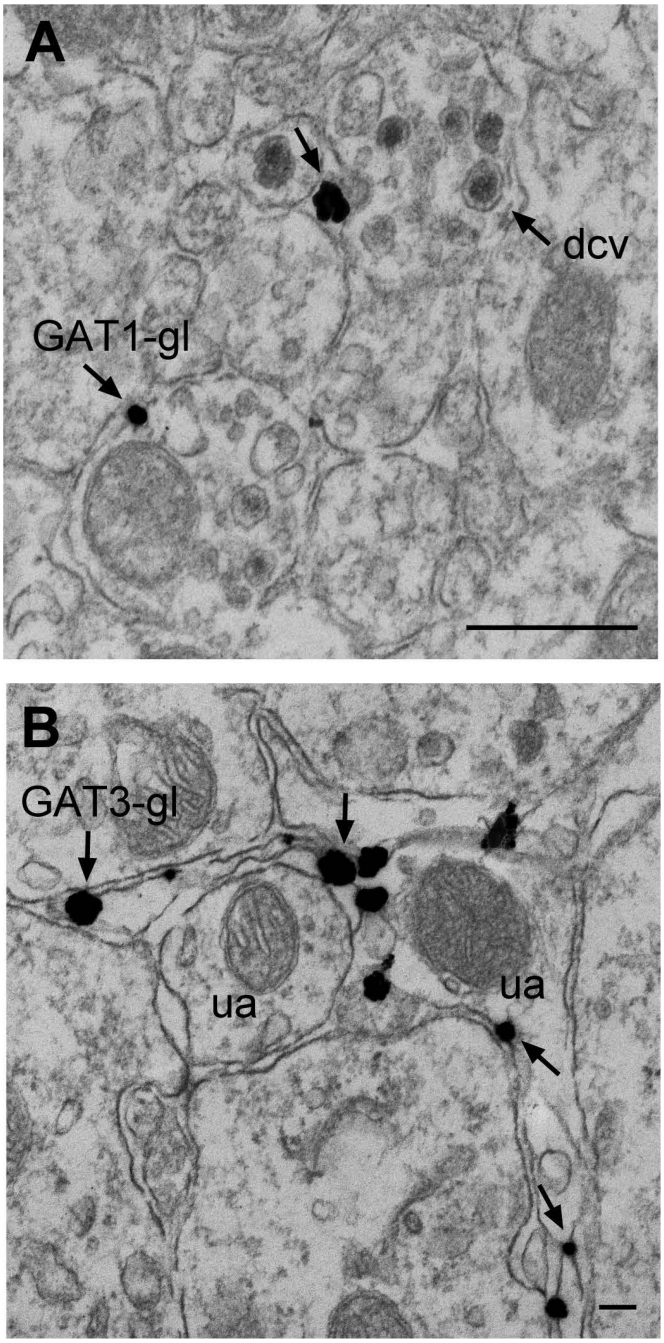

Figure 9. GAT1- and GAT3-ir glial processes are closely associated with unmyelinated axons

A. GAT1-ir glial processes surround axon bundles that include unmyelinated axons and an axonal process that contains small clear vesicles and dense core vesicles (dcv). Arrows – immunogold labeling. B. Immunogold particles (arrows) are closely associated with the membranes of GAT3-ir glial cells surrounding unmyelinated axons (ua). Scale bars 500 nm.

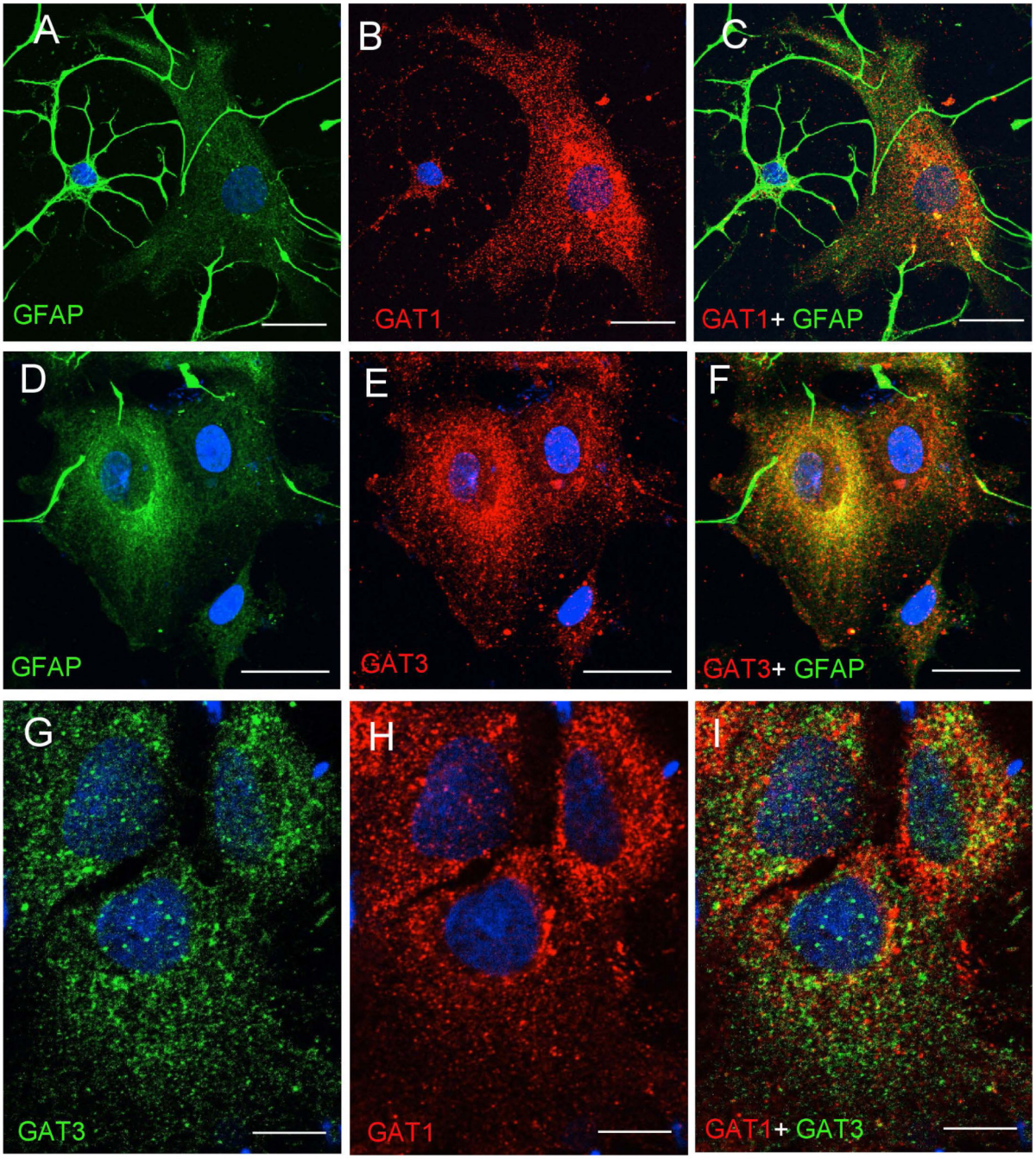

Figure 10. GAT1 and GAT3 are expressed in GFAP-immunopositive astrocytes

A - I. Glial cells in SCN cell cultures were stained for the presence of GAT1, GAT3, and GFAP. The images were taken from one-week old cultures. A - C. GFAP-positive (green) astrocytes were immunoreactive for GAT1 (red), 100×. C. The images shown in A and B were merged. D - F. GFAP-positive astrocytes were also immunoreactive for GAT3 (red), 60×. F. The GFAP and GAT3 images shown in D and E were merged. A – F. scale bar 25 μm. G – I. Co-expression of GAT1 and GAT3 in glial cells (presumably astrocytes), scale bar 10 μm. The GAT1 and GAT3 images were merged.

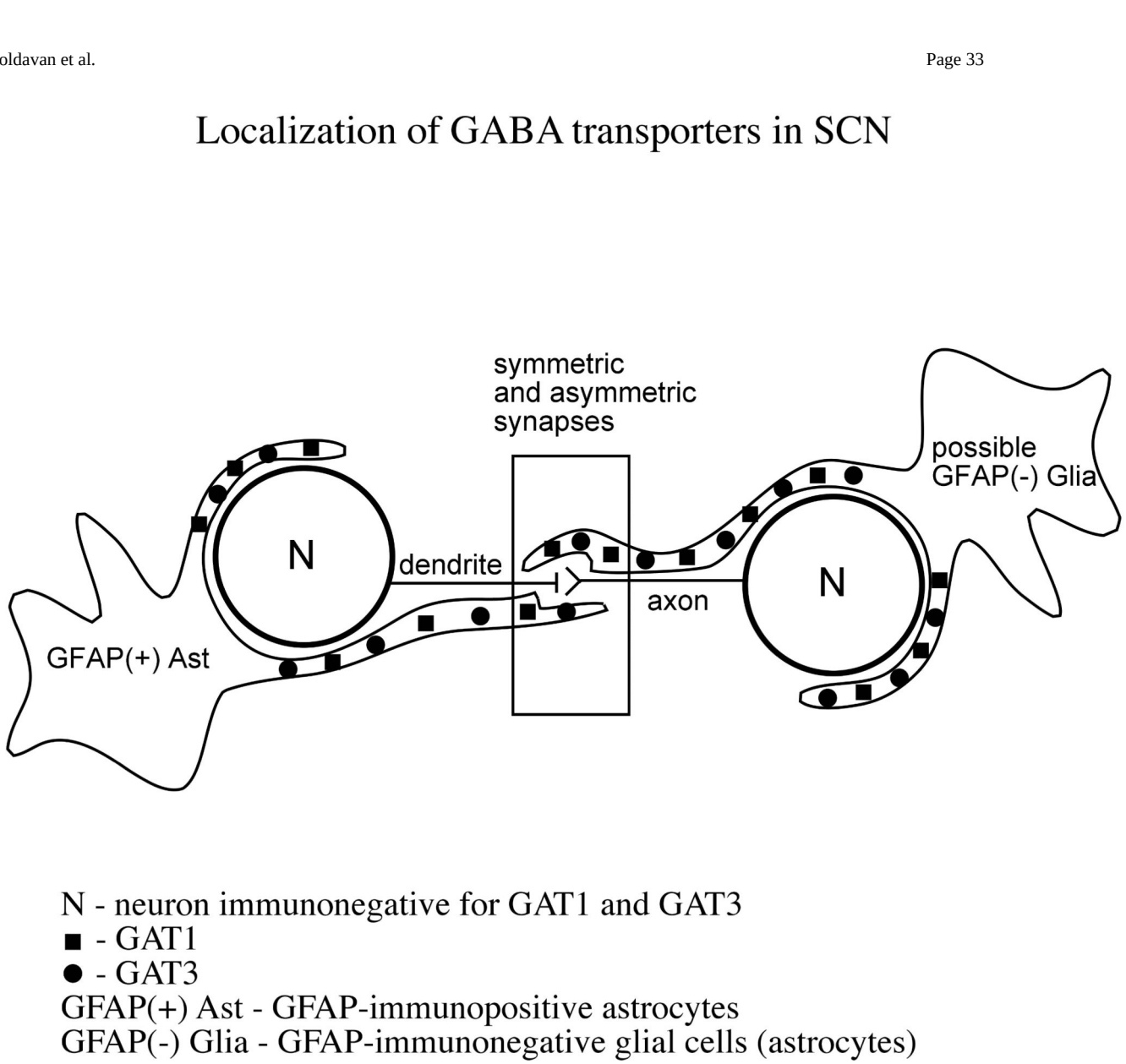

Figure 11. Schematic model of the location of GATs in SCN

This model schematically proposes that GAT1 and GAT3 are expressed in the distal processes of GFAP-positive astrocytes, and also by GFAP-negative glial cells. The model shows that GATs-ir processes of glial cells surround neuronal cell bodies and axo-dendritic synapses. The location of the GATs suggests they can restrict GABA diffusion from the synapses and regulate extracellular GABA concentration around the neuronal cell bodies.

Table 1

Primary and secondary antibodies used in the present studies.

Primary antibody						**Corresponding secondary antibody**
Antiserum	**Host**	**Antigen (Immunogen)**	**Description (Specification)**	**Code & Vendor (Manufacturer)**	**Method & Dilution**	**Name, method, dilution**
Anti-GAT1	Rabbit	Peptide (C)ERNMHQ MTDGLDK, corresponding to amino acids residues 194-206 of rat GAT1 (Accession P23978). 2nd extracellular loop.	Extracellular domain, affinity purified polyclonal antibody, *SLC6A1;* supplied with control antigen to GAT1 (blocking peptide)	AGT-001 Alomone[2]	WB; 1:500; 1:1000 with blocking peptide	WB; 1:5000, donkey polyclonal anti-rabbit IgG-HRP, sc-2313, Santa Cruz[9]
Anti-GAT1	Rabbit	C-terminus of rat GAT1 (aa 588-599)	Affinity purified polyclonal antibody	AB1570 Millipore[5]	IHC; 1:100	IHC; 1:100, donkey-anti-rabbit IgG DyLight 549 (#711-505-152), Jackson[4]
Anti-GAT1	Rabbit	Peptide corresponding to amino acid residues from the C-terminal region of rat GAT1	Affinity purified polyclonal IgG antibody, detects a band of approximately 67 kDa; *SLC6A1*	ab72448 Abcam[1]	IHC; 1:500 EM; 1:50	IHC; 1:500, donkey anti-rabbit IgG DyLight 594 preadsorbed, ab96921, Abcam[1]
Anti-GAT1	Rabbit	20 residue C-terminal synthetic peptide (Rat)	polyclonal antibody, reacts specifically with a 72 kDa protein; *SLC6A1*	ab426 Abcam[1]	IHC; 1:1000	IHC; 1:500, donkey anti-rabbit IgG DyLight 594 preadsorbed, ab96921, Abcam[1]
Anti-GAT3	Rabbit	C-terminus of rat GAT3 (aa 607-627) coupled to KLH	Affinity purified polyclonal antibody	AB1574 Millipore[5]	WB; 1:1000 IHC; 1:100, 1:500 EM; 1:50	WB; 1:4000, IRDye 680 Goat Anti-Rabbit IgG (#926-32221),LI-COR[6] IHC; 1:100, donkey-anti-rabbit IgG DyLight 488 (#711-485-152), Jackson[4] IHC; 1:500, donkey anti-rabbit IgG DyLight 594 preadsorbed, ab96921, Abcam[1]
Anti-GAT3	Mouse	C-terminus of rat GAT3 (aa 601-625)	Monoclonal [B-6] IgG_{2b}	sc-376001, Santa Cruz[9]	IHC; 1:1000	IHC; 1:500, Donkey Anti-Mouse IgG Alexa Fluor 488, (#715-546-151), Jackson[4]
Anti-GAPDH	Mouse	Glyceraldehyde-3-phosphate dehydrogenase from rabbit muscle	Purified monoclonal antibody, clone 6C5, recognizes a 36 kDa band of the reduced monomer	MAB374 Millipore[5]	WB; 1:8000	WB; 1:200000, Rabbit polyclonal anti-mouse IgG-HRP, AP160P, Millipore[3] WB; 1:3000, IRDye 800CW Goat Anti-Mouse IgG (#926-32210), LI-COR[6]

Primary antibody						Corresponding secondary antibody
Antiserum	**Host**	**Antigen (Immunogen)**	**Description (Specification)**	**Code & Vendor (Manufacturer)**	**Method & Dilution**	**Name, method, dilution**
Anti-GFAP	Mouse	Purified glial filament (Debus, E., 1983)	Purified monoclonal antibody, clone GA5	MAB3402 Millipore[5]	IHC (slices); 1:500 IHC (cell culture); 1:500	IHC; 1:500, Donkey Anti-Mouse IgG Alexa Fluor 488, (#715-546-151), Jackson[4]
Anti-NFH	Hen	Purified IgY fractions from eggs	Purified neurofilament protein (200 kDa)	NFH AVES[3]	IHC; 1:500	IHC; 1:500, Donkey Anti-Chicken IgY CF488A, SAB4600031-50, Sigma-Aldrich[10]
Anti-NeuN	Mouse	Purified cell nuclei from mouse brain	Purified monoclonal antibody, clone A60, IgG conjugated to Alexa Fluor®488	MAB377X Millipore[5]	IHC; 1:500	
Anti-NSE	Rabbit	Synthetic peptide derived from human NSE	Affinity purified polyclonal to NSE antibody	ab53025 Abcam[1]	IHC; 1:500	IHC; 1:500, Donkey Anti-Rabbit IgG DyLight 594 preadsorbed, ab96921, Abcam[1]
Anti-AVP	Guinea pig	Synthetic peptide as the immunogen, epitope has not been mapped	Anti-(Arg[8])-Vasopressin, undiluted, lyophilized polyclonal not purified antiserum,	S-3100 Peninsula[8]	IHC; 1:2000	IHC; 1:500, Goat Anti-Guinea Pig IgG Alexa Fluor 594, (A-11076), Life Technologies[7]
Anti-VIP	Rabbit	Full length protein VIP (Pig) conjugated to Bovine thyroglobulin by a CDI linker	Whole antiserum polyclonal IgG	ab43841 Abcam[1]	IHC; 1:250	IHC; 1:500, Donkey Anti-Rabbit IgG DyLight 594 preadsorbed, ab96921, Abcam[1]

[1] Abcam Inc., Cambridge, MA

[2] Alomone Labs Ltd., Jerusalem, Izrael

[3] Aves Labs, Tigard, OR

[4] Jackson ImmunoResearch Laboratories, Inc., West Grove, PA

[5] Millipore (Chemicon), Temecula, CA

[6] LI-COR Biosciences, Lincoln, NE

[7] Life Technologies, Grand Island, NY

[8] Peninsula Laboratories International Inc., San Carlos, CA

[9] Santa Cruz Biotechnology Inc., CA

[10] Sigma-Aldrich, Saint Louis, MO